

# AN ANALYTIC FORMULATION OF 21-CM SIGNAL FROM EARLY PHASE OF EPOCH OF REIONIZATION

JANAKEE RASTE<sup>1,\*</sup> AND SHIV SETHI<sup>1</sup>

<sup>1</sup>*Raman Research Institute, Bangalore 560080, India*

## ABSTRACT

We present an analytic formulation to model the fluctuating component of the H I signal from the epoch of reionization during the phase of partial heating. During this phase, we assume self-ionized regions, whose size distribution can be computed using excursion set formalism, to be surrounded by heated regions. We model the evolution of heating profile around these regions (near zone) and their merger into the time-dependent background (far zone). We develop a formalism to compute the two-point correlation function for this topology, taking into account the heating auto-correlation and heating-ionization cross-correlation. We model the ionization and X-ray heating using four parameters: efficiency of ionization,  $\zeta$ , number of X-ray photons per stellar baryon,  $N_{\text{heat}}$ , the spectral index of X-ray photons,  $\alpha$ , and the minimum frequency of X-ray photons,  $\nu_{\text{min}}$ . We compute the H I signal in the redshift range  $10 < z < 20$  for the  $\Lambda$ CDM model for a set of these parameters. We show that the H I signal for a range of scales 1–8 Mpc show a peak strength  $100\text{--}1000 (\text{mK})^2$  during the partially heated era. The redshift at which the signal makes a transition to uniformly heated universe depends on modelling parameters, e.g. if  $\nu_{\text{min}}$  is changed from 100 eV to 1 keV, this transition moves from  $z \simeq 15$  to  $z \simeq 12$ . This result, along with the dependence of the H I signal on modelling parameters, is in reasonable agreement with existing results from N-body simulations.

*Keywords:* cosmology: theory —dark ages, reionization, first stars

\* Joint Astronomy Program, Indian Institute of Science, Bangalore 560012, India

## 1. INTRODUCTION

The probe of the epoch of reionization remains one of the outstanding aims of modern cosmology. In the past 15 years, important strides have been made in this direction, mainly led by the detection of Gunn-Peterson effect at  $z \simeq 6$  and the CMB temperature and polarization anisotropy detections by WMAP and Planck (Ade et al. (2014); Hinshaw et al. (2013); Ade et al. (2015); Fan et al. (2000); Becker et al. (2001)). The former discovery suggests that the universe could be making a transition from neutral to fully ionized at  $z \simeq 6$ , while the latter shows the universe might have been fully ionized at  $z \simeq 8.5$ . The current best bounds on the reionization optical depth from Planck put stringent constraints on the redshift of reionization:  $z_{\text{reion}} = 8.5 \pm 1$  (Ade et al. (2015)).

One important missing piece in these probes is that neither seem capable of discerning the dynamics of the reionization process. For instance, the CMB anisotropies (both polarization and temperature) are sensitive only to the integrated optical depth through the surface of reionization (e.g. Dodelson (2003)).

Theoretical estimates suggest that dark age of the universe might have ended around  $z \simeq 30$  with the formation of first structures in the universe. These structures are expected to emit UV light which might have reionized the universe at  $z \simeq 9$  (see e.g. Barkana & Loeb (2001); Pritchard & Loeb (2012); Natarajan & Yoshida (2014); Morales & Wyithe (2010) and references therein). The most direct way to probe this transition is through the detection of redshifted hyperfine 21 cm line of neutral hydrogen (H I). The past one decade has seen major progress on both theoretical and experimental front in this endeavour. Currently, there are many ongoing experiments that are attempting to detect both the global H I signal and its fluctuating component from the epoch of reionization. The H I signal from the epoch has been computed both analytically and using numerical simulations. Theoretical estimates show that the global signal is observable in both absorption and emission with its strength in the range  $-200$ – $20$  mK in a frequency range of  $50$ – $150$  MHz, which corresponds roughly to a redshift range  $25 > z > 8$  (e.g. Madau et al. (1997); Tozzi et al. (2000); Gnedin & Shaver (2004); Sethi (2005)). The fluctuating component of the signal is likely to be an order of magnitude smaller on scales in the range  $3$ – $100$  Mpc, which implies angular scales in the range  $\simeq 1$ – $30$  arc-minutes (e.g. Zaldarriaga et al. (2004); Furlanetto et al. (2004a,b); Pritchard & Furlanetto (2007); for comprehensive reviews see e.g. Pritchard & Loeb (2012); Natarajan & Yoshida (2014); Morales & Wyithe (2010)). Many of the ongoing and upcoming experiments have the capability to detect this signal in hundreds of hours of integration (e.g. Ahn et al. (2015a); Mesinger et al. (2014)). Upper limits on the fluctuating component of the H I signal have been obtained by many ongoing experiments—GMRT, MWA, PAPER, and LOFAR (Patil et al. (2017); Beardsley et al. (2016); Ali et al. (2015); Paciga et al. (2013)). The best current upper limits corresponds to:  $k^3 P(k)/(2\pi^3) < (22.4 \text{ mK})^2$  for  $0.15 < k < 0.5 \text{ hMpc}^{-1}$  at  $z \simeq 8.4$  (Ali et al. (2015)).

The H I signal carries crucial information about the first sources in the universe. In particular, the H I signal is determined by the radiation emitted by these sources in three frequency bands: UV radiation that ionizes the medium, Lyman- $\alpha$  radiation (frequencies between Lyman-limit and Lyman- $\alpha$ ), and X-ray photons (all photons with energies much higher than hydrogen and helium ionization threshold). The emission in these three bands determines the evolution of the global H I signal. And, along with primordial density perturbations given by the  $\Lambda$ CDM model, the perturbations of these radiation fields establish the length scales of the fluctuating component of the signal.

In this paper, our main focus is the analytic modelling of the fluctuating component of the H I signal in its early phase when the universe is partially heated. This phase of the EoR has been extensively studied using numerical methods and analytic estimates (e.g. Pritchard & Furlanetto (2007); Tashiro & Sugiyama (2013); Mesinger et al. (2013); Fialkov et al. (2014); Ghara et al. (2015); Pacucci et al. (2014); Fialkov et al. (2017); Visbal et al. (2012); Mesinger et al. (2011)). We present a new formalism in this paper which seeks to unravel the correlation structure of the fluctuations based on the topology of the ionization and heating regions.

In the next section, we review the H I signal from the epoch of reionization and discuss the impact of three radiation fields on the signal. In particular, the modelling of X-ray heating is described in detail. In section 3, we present our formalism for computing the two-point correlation function of the H I signal. We also discuss various approximations, assumptions, and limits germane to our formulation. In section 4, we present our results and compare them with the inferences of other studies. In section 5 we summarize our findings and make concluding remarks. Throughout this paper, we assume the spatially-flat  $\Lambda$ CDM model with the following parameters:  $\Omega_m = 0.254$ ,  $\Omega_B = 0.049$ ,  $h = 0.67$  and  $n_s = 0.96$ , with the overall normalization corresponding to  $\sigma_8 = 0.83$  (Ade et al. (2015)).

## 2. COSMIC DAWN AND EPOCH OF REIONIZATION

In the rest frame, hyperfine splitting of the ground state of neutral hydrogen causes an energy difference that corresponds to a wavelength  $\lambda = 21.1$  cm. The excitation temperature of this line,  $T_S$ , is determined by three processes in early universe: emission and absorption of CMB photons which is a blackbody of temperature  $T_{\text{CMB}}$ , collisions with atoms, and the mixing of the two levels caused by Lyman- $\alpha$  photons (Wouthuysen-Field effect).  $T_S$  can be expressed in terms of the colour temperature of Lyman- $\alpha$  photons,  $T_\alpha$ , gas kinetic temperature  $T_K$ , and  $T_{\text{CMB}}$  (Field (1958); Pritchard & Loeb (2012)):

$$T_S = \frac{T_{\text{CMB}} + y_\alpha T_\alpha + y_c T_K}{1 + y_\alpha + y_c} \quad (1)$$

Here  $y_c \propto n_H$  and  $y_\alpha \propto n_\alpha$  ( $n_H$  and  $n_\alpha$  are the number densities of neutral hydrogen atoms and Lyman- $\alpha$  photons, respectively) determine the efficiency of collisions and Lyman- $\alpha$  photons, respectively. In the early universe,  $1000 < z < 100$ ,  $T_S$  relaxes to  $T_{\text{CMB}}$ . In the redshift range  $100 < z < 30$ , collisions determine the spin temperature and  $T_S$  relaxes to the kinetic temperature  $T_K$  of the matter. As the epoch of reionization commences, the production of Lyman- $\alpha$  photons couples the spin temperature to the colour temperature of Lyman- $\alpha$   $T_\alpha$ . It can be shown that multiple scattering of Lyman- $\alpha$  photons with H I causes  $T_\alpha$  to relax to the kinetic temperature (e.g. Chen & Miralda-Escudé (2004); Field (1959); Rybicki & dell’Antonio (1994)). Therefore if  $y_{\text{tot}} = y_c + y_\alpha \gtrsim T_{\text{CMB}}/T_K$ , then  $T_S$  is strongly coupled to  $T_K$ . Otherwise, it relaxes to  $T_{\text{CMB}}$ .

The H I emits or absorbs 21-cm radiation from CMB depending on whether its  $T_S$  is greater than or less than  $T_{\text{CMB}}$ . This temperature difference is observable and can be expressed as (e.g. Pritchard & Loeb (2012); Madau et al. (1997); Shaver et al. (1999); Gnedin & Shaver (2004); Sethi (2005)):

$$\begin{aligned} \Delta T_b &= \frac{1 - e^{-\tau}}{1 + z} (T_S - T_{\text{CMB}}) \\ &\simeq \frac{\tau}{1 + z} (T_S - T_{\text{CMB}}) \\ &\simeq 26.25 \, n(1 + \delta) \left(1 - \frac{T_{\text{CMB}}}{T_S}\right) \left(\frac{1 + z}{10} \frac{0.14}{\Omega_m h^2}\right)^{\frac{1}{2}} \left(\frac{\Omega_b h^2}{0.022}\right) \text{mK} \end{aligned} \quad (2)$$

Here we ignore redshift space distortion. In writing the expression, we have expressed the H I number density as,  $n_H = \bar{n}_H n(1 + \delta)$ ;  $\delta$  corresponds to density inhomogeneities in the gas. The value of mean density  $\bar{n}_H$  has been absorbed in the prefactor of Eq. (2). In our formulation every small volume is either completely neutral or completely ionized, therefore we define a variable  $n$  which is unity if the medium is neutral and zero otherwise. In addition to density inhomogeneities, there are ionization and spin temperature,  $T_S$ , inhomogeneities (as the medium is partially ionized or partially heated). We further define dimensionless temperature fluctuation as (Zaldarriaga et al. (2004)):

$$\begin{aligned} \psi &= n(1 + \delta) \left(1 - \frac{T_{\text{CMB}}}{T_S}\right) \\ &= n(1 + \delta)(1 - s) \end{aligned} \quad (3)$$

We have defined  $s = T_{\text{CMB}}/T_S$ . The statistics of  $\psi$  allows us to study the main physical processes that cause brightness temperature fluctuations:  $\delta$  (density perturbations),  $n$  (ionization inhomogeneities) and  $s$  (fluctuations of kinetic temperature). All these quantities are functions of position in space but we suppress this dependence for notational clarity. In this paper, we assume  $T_\alpha = T_K$  everywhere, as discussed in section 2.3.

We next consider the impact of the three radiation fields—ionizing radiation, Lyman- $\alpha$  photons, and X-ray photons—on the brightness temperature inhomogeneities.

### 2.1. Photo-ionization

At the end of the dark ages, high density regions of the universe collapse and form structures of different masses. In our work we assume that the smallest mass that can collapse corresponds to H I-cooled halo (e.g. Barkana & Loeb (2001)):

$$M_{\text{min}} = 3.915 \times 10^8 \frac{\Omega_m^{1/2}}{h(1 + z)^{3/2}} M_\odot \quad (4)$$

These collapsed structures emit UV photons, which are absorbed in the immediate vicinity of the sources and carves out H II regions around them in the IGM. These structures also emit Lyman- $\alpha$  and X-rays radiation which penetrates further into the IGM.

The size distribution of the ionization bubbles can be computed using excursion set formalism by defining self-ionized regions (Furlanetto et al. (2004a)). These regions have enough sources to ionize all the gas in it. Such regions are not created by a single source but rather a set of highly clustered sources which is the case in the early universe for  $\Lambda$ CDM model, and therefore these regions are larger than the H II regions of a single source. Here we briefly describe the formalism (for details see e.g. Furlanetto et al. (2004a) and references therein). We start by defining  $\zeta$ , the ionization efficiency factor:

$$\zeta = f_{\star} f_{\text{esc}} N_{\text{ion}} N_{\text{rec}}^{-1} \quad (5)$$

Here  $f_{\star}$  is the fraction of collapsed baryons that is converted into stars.  $f_{\text{esc}}$  equals the fraction of ionizing photons that escape the source halo and  $N_{\text{ion}}$  is number of hydrogen ionizing (UV) photons created per stellar baryon while  $N_{\text{rec}}$  is the number of recombinations. We assume  $\zeta$  to be constant in this paper, even though it could be time dependent owing to the evolution of quantities used to define it. Inside a self-ionization region,  $1/\zeta = f_{\text{coll}} = M_{\text{coll}}/M_{\text{tot}}$ , where  $f_{\text{coll}}$  is the fraction of collapsed mass inside the self-ionized region.

Using the extended Press-Schechter model, the collapse fraction can be expressed as,

$$f_{\text{coll}} = \text{erfc} \left[ \frac{\delta_c(z) - \delta_m}{\sqrt{2[\sigma_{\text{min}}^2 - \sigma^2(m)]}} \right]$$

Here  $\sigma^2(m)$  is the variance of density fluctuations for mass  $m$ , the mass of the self-ionized region at  $z = 0$ ;  $\sigma_{\text{min}}^2 \equiv \sigma^2(m_{\text{min}})$  and  $\delta_c(z) = 1.68/D_+(z)$  is the critical density for collapse at redshift  $z$  and  $D_+$  is the growing mode of density perturbations.  $\delta_x(m, z)$  is the redshift and mass dependent barrier for excursion set formalism. The linear fit to this true barrier at  $m \rightarrow \infty$  is,

$$B(m, z) = \delta_c(z) - \sqrt{2} K(\zeta) \sigma_{\text{min}} + \frac{K(\zeta) \sigma^2(m)}{\sqrt{2} \sigma_{\text{min}}}$$

$K(\zeta) = \text{erf}^{-1}(1 - \zeta^{-1})$ . To find the self-ionized region, we need to find the first up-crossing of  $\delta$  above the curve described by  $B(m, z)$ . We can write the mass function analytically as (Sheth (1998)),

$$m \frac{dn}{dm} = \sqrt{\frac{2}{\pi}} \frac{\bar{\rho}}{m} \left| \frac{d \ln \sigma}{d \ln m} \right| \frac{B_0}{\sigma(m)} \exp \left[ -\frac{B^2(m, z)}{2\sigma^2(m)} \right] \quad (6)$$

Where  $B_0 \equiv \delta_c(z) - \sqrt{2} K(\zeta) \sigma_{\text{min}}$  is the value of barrier at  $m \rightarrow \infty$ . Eq. (6) gives the comoving number density of self-ionized bubbles in the mass range  $(m, m + dm)$ . Here  $\bar{\rho}$  is the background mass density. We use  $\Lambda$ CDM power spectrum (the matter power spectrum of the  $\Lambda$ CDM model is generated using publicly-available code CMBFAST) for solving Eq. (6). We note that this formalism has been used extensively for analytic work and for simulations of epoch of reionization, including in the publicly-available code 21cmFAST (Mesinger et al. (2011)). In a numerical simulation, the self-ionized region is constructed by identifying the largest contiguous region that satisfies the condition for a self-ionized bubble:  $f_{\text{coll}} = 1/\zeta$ . This region need not be spherical. For analytic work, we assume the region to be spherical. We discuss the implications of this assumption in a later section.

Figure 1 shows the effect of  $\zeta$  on the global ionization fraction  $f_i$  of the universe. For higher value of  $\zeta$ , the reionization is completed at higher redshift. In Figure 2 we show the distribution of volume fraction occupied by bubbles of different sizes and its evolution with redshift. We show the volume fraction as a function of halo mass, which can be related to the comoving size of the self-ionized bubble as:  $R_x \simeq 0.09 \text{ Mpc} (M/10^8 M_{\odot})^{1/3} \zeta^{1/3}$ . Figure 2 agrees with the results of Furlanetto et al. (2004a) (their Figure 2) for the set of parameters used by them. For the set of parameters used in this paper, the self-ionized bubbles are smaller, e.g. at  $z = 12$  the peak of the bubble distribution corresponds roughly to a scale of  $R_x \simeq 10 \text{ Mpc}$  for Furlanetto et al. (2004a), while it peaks at  $R_x \simeq 3 \text{ Mpc}$  for our case.

## 2.2. X-Ray Heating

Photons of energy  $E \gg 13.6 \text{ eV}$  are not absorbed in the H II region but escape into the surrounding medium. These photons ionize and heat the medium through photoionization and secondary collisional ionization and excitation.

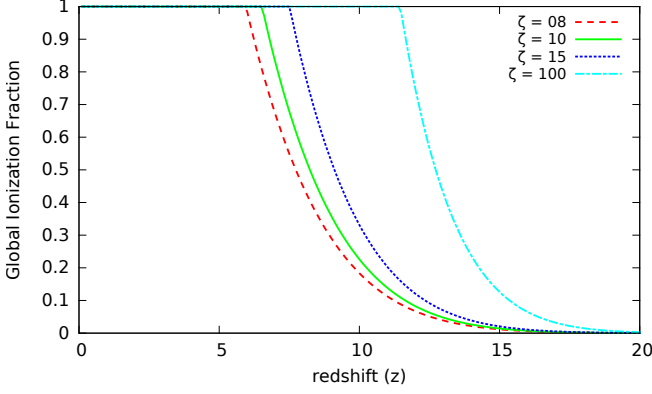


**Figure 1.** Evolution of global ionization fraction ( $f_i$ ) is shown for different values of  $\zeta$ .

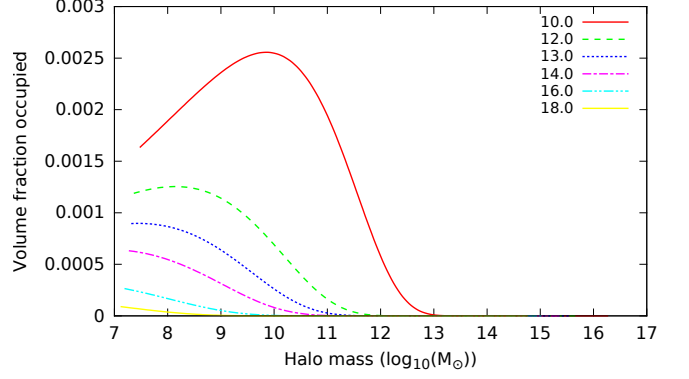


**Figure 2.** Evolution of the size distribution of self-ionized regions as a function of halo mass is shown for  $\zeta = 10$ .

These photons can ionize the medium to a level less than 10% and can impart up to 20% of their total energy into heating the medium (e.g. [Shull & van Steenberg \(1985\)](#); [Venkatesan et al. \(2001\)](#)). As the fraction of ionization in this process is generally tiny, in our study, we assume the medium outside the ionized region to be comprised of neutral hydrogen and neutral helium with primordial abundances.

A key fact in X-ray heating of the mostly neutral gas outside the H II region is that photoionization cross section falls as  $1/\nu^3$  for energies far larger than the threshold energy. As the low energy X-ray photons are absorbed with higher probability, they contribute to heating the medium immediately surrounding the H II region whereas the higher energy photons free-stream through the medium. As they are redshifted, their probability of absorption slightly increases. These photons uniformly heat up the whole IGM to some background temperature  $T_{bg}$ .

In this section, we calculate the profile of kinetic temperature around self-ionized regions. In our analysis we separate the regions into near- and far-zones. In the near zone the heating is dominated by X-ray photons from an individual self-ionized region. In the far zone, the contribution from only the far away background sources is taken into account.

### 2.2.1. Near Zone

To compute the temperature profile for an individual source at a redshift  $z$ , we calculate the total energy absorbed (over the entire history of the source) by a point close to the source at redshift  $z'$ . In this subsection and the following one, primed quantities are calculated at the receiving point (point  $P$ ), unprimed quantities are at the source (point  $S$ ), and quantities with 0 subscript are comoving quantities.

The energy attained by electrons due to ionization of species  $i$  (here  $i$  runs over hydrogen and neutral helium with their relative fractions  $x_i = 12/13$  and  $1/13$  of the baryon number, respectively), per unit time, per unit comoving volume, per unit frequency (at  $P$ ) is:

$$\frac{dE'_{\nu'}(i)}{dt'd\nu'dV_0} = (h\nu' - h\nu_i) \frac{dN'_{\nu'}}{dt'd\nu'dV_0} P(i, \nu') \quad (7)$$

Here  $dN'_{\nu'}/(dt'd\nu'dV_0)$  is the number of X-ray photons (of frequency  $\nu'$ ) received per unit time per unit frequency per unit comoving volume and  $P(i, \nu')$  gives the probability of ionization of species  $i$  by a photon of frequency  $\nu'$  in a shell of thickness  $d\nu'$ :

$$P(i, \nu') = n'_i \sigma_i(\nu') d\nu' \quad (8)$$

Here  $n'_i = x_i n_0 (1 + z')^3$  is the local number density of species  $i$ , and  $\sigma_i(\nu')$  is the ionization cross section of an atom by an X-ray photon of frequency  $\nu'$ <sup>1</sup>:

$$\sigma_i(\nu') = \sigma_{i0} \left( \frac{\nu'}{\nu_i} \right)^{-3}, \quad (9)$$

<sup>1</sup> We use here the approximate expressions for the frequency dependence of the ionization cross-section of hydrogen and neutral helium; for more precise formulas see e.g. [Osterbrock \(1989\)](#). Our results are not affected by this choice.

with  $\nu_i$  being the ionization threshold of species  $i$ . We assume the X-ray photon luminosity to be given by a power law (e.g. [Mesinger et al. \(2011\)](#) and references therein):

$$\dot{N}_\nu = \dot{N}_t \left( \frac{\nu}{\nu_{\min}} \right)^{-\alpha} \quad (10)$$

where  $\nu_{\min}$  is the lowest frequency (in the rest frame of the source) of X-ray photons escaping from ionizing sources. We also have,

$$\frac{d\dot{N}'_{\nu'}}{d\nu'} = \frac{d\dot{N}_\nu}{d\nu} e^{-\tau(R_0, \nu')} \quad (11)$$

The optical depth between two point separated by comoving distance  $R_0$  is given by:  $\tau(R_0, \nu') = \int \sum_i P(i, \nu')$ .

We calculate the X-ray luminosity of a self-ionized region following the prescription of the last section, which allows us to relate  $\dot{N}_t$  to  $\zeta$  (Eq. (5)) and the comoving radius of the self-ionized region  $R_x$ :

$$\begin{aligned} \dot{N}_t &= \frac{\text{Number of X-ray photons emitted}}{\text{time}} \\ &= \frac{\text{Number of X-rays emitted}}{\text{Number of Baryons in stars}} \frac{\text{Number of Baryons in stars}}{\text{Number of Collapsed Baryons}} \frac{\text{Number of Collapsed Baryons}}{\text{Time}} \\ &= N_{\text{heat}} f_\star \frac{d(N_{\text{halo}} f_{\text{coll,ion}})}{dt} \end{aligned} \quad (12)$$

where  $N_{\text{heat}}$  is the number of X-ray photons emitted per stellar baryons.  $f_\star$  is the fraction of collapsed baryons that is converted into stars.  $N_{\text{halo}} = 4\pi/3 R_x^3 n_0$  is the number of baryons in a self-ionized region of radius  $R_x$ .  $f_{\text{coll,ion}} = 1/\zeta$  is the collapsed fraction in an ionized region. We further assume that the collapsed fraction inside an ionization region follows the global collapsed fraction,  $f_{\text{coll,g}}$ , which we obtain from the excursion set formalism. This gives us:

$$\frac{d(N_{\text{halo}} f_{\text{coll,ion}})}{dt} = \frac{1}{\zeta} N_{\text{halo}} \frac{\dot{f}_{\text{coll,g}}}{f_{\text{coll,g}}} \quad (13)$$

Using Eqs. (7) to (13), using  $dV_0 = 4\pi R_0^2 dR_0$ , adding contribution due to all the species and integrating over all the frequencies  $\nu > \nu_{\min}$ , we get the energy that goes into heating the medium per unit time per unit volume:

$$\frac{dE'_{\text{heat}}}{dt' dV_0} = \frac{h f_H \alpha N_{\text{heat}} f_\star n_0^2 \nu_{\min}^\alpha}{3\zeta} \frac{R_x^3}{R_0^2} \frac{(1+z')^{\alpha+3}}{(1+z)^{\alpha+1}} \frac{\dot{f}_{\text{coll,g}}}{f_{\text{coll,g}}} \int_{\nu'_{\min}}^{\infty} \nu'^{-\alpha-4} e^{-\tau(R_0, \nu')} \sum_i (\nu' - \nu_i) x_i \sigma_{i0} \nu_i^3 d\nu' \quad (14)$$

Where,  $\nu'_{\min} = \nu_{\min}(1+z')/(1+z)$  is the minimum frequency from the source that reaches P. We assume that  $f_H = 0.15$  is the fraction of energy of emitted photoelectron that goes into heating the medium ([Shull & van Steenberg \(1985\)](#), [Venkatesan et al. \(2001\)](#)).

Eq. (14) gives the energy that goes into heating the medium by X-ray photons per unit time per unit comoving volume at distance  $R_0$  from the center of a self-ionized bubble of radius  $R_x$ . To get the total increase in temperature due to this heating, we need to integrate this over time. If  $z'_c$  is the redshift at which we compute the heating profile, then to take into account the adiabatic cooling since higher redshift  $z'$ , we multiply by  $(1+z'_c)^2/(1+z')^2$ . We neglect all other cooling processes.  $R_x(t')$ , the radius of the given ionization region at time  $t'$  in the past, is not a straightforward quantity to calculate as excursion set formalism doesn't give the time evolution of the radius of a particular self-ionized region. Given that the formalism allows us to compute the evolution of the average ionized fraction  $f_i$ , we assume  $R_x^3(t') = R_x^3(t)(f_i(t')/f_i(t))$ . This gives,

$$\begin{aligned} \frac{dE'_{\text{heat}}}{dV_0} &= \frac{h f_H \alpha N_{\text{heat}} f_\star n_0^2 \nu_{\min}^\alpha}{3\zeta} \frac{R_x^3}{R_0^2} (1+z'_c)^2 \\ &\quad \int_{t(z_c)}^{t(z_0)} dt' \frac{f_i(t')}{f_i(t)} \frac{\dot{f}_{\text{coll,g}}}{f_{\text{coll,g}}} \left( \frac{1+z'}{1+z} \right)^{\alpha+1} \\ &\quad \int_{\nu'_{\min}}^{\infty} d\nu' \nu'^{-\alpha-4} e^{-\tau(R_0, \nu')} \sum_i (\nu' - \nu_i) x_i \sigma_{i0} \nu_i^3 \end{aligned} \quad (15)$$

Finally, this allows us to compute the increase in temperature due to a self-ionized region of radius  $R_x$  at a distance  $R_0$  from the center of the ionized region:

$$\begin{aligned}\Delta T' &= \frac{1}{n_0 k_B} \frac{dE'_{\text{heat}}}{dV_0} \\ &= \frac{h f_H \alpha N_{\text{heat}} f_{\star} n_0 \nu_{\min}^{\alpha}}{3 k_B \zeta} \frac{R_x^3}{R_0^2} (1 + z'_c)^2 \\ &\quad \int_{t(z_{\star})}^{t(z_0)} dt' \frac{f_i(t')}{f_i(t)} \frac{\dot{f}_{\text{coll,g}}}{f_{\text{coll,g}}} \left( \frac{1 + z'}{1 + z} \right)^{\alpha+1} \\ &\quad \int_{\nu'_{\min}}^{\infty} d\nu' \nu'^{-\alpha-4} e^{-\tau(R_0, \nu')} \sum_i (\nu' - \nu_i) x_i \sigma_{i0} \nu_i^3\end{aligned}\tag{16}$$

We can estimate the typical energies of photons that are absorbed close to the source: at  $z = 20$ , for  $\nu \simeq 100$  eV, the photon is absorbed at a comoving distance  $\simeq 3$  Mpc from the source while a photon of 1 keV is absorbed at  $\simeq 300$  Mpc. Therefore, the low energy photons are absorbed locally and determine the heating profile of the near zone while the high energy photons play the role of determining the evolution of the average temperature which we discuss next. One can compute the optical depth of high energy photons to determine the fraction of these photons that are absorbed until the epoch of interest; for  $\nu = 2$  keV, nearly 80% of the photons emitted at  $z = 20$  remain unabsorbed at  $z = 15$ . This means that some of these photons are absorbed neither locally nor do they participate in heating in the far zone; we return to this point in the next sub-section. We also note that X-ray photons are not absorbed within the H II region and hence the effective length for computing the optical depth is not  $R_0$  but  $R_0 - R_x$ , which we take into account in our numerical computation.

### 2.2.2. Far Zone

In the far zone, multiple sources contribute to the heating at any point. As noted above, low frequency X-ray photons are preferentially absorbed close to the ionizing region in the near zone (Eq. (8)), while higher frequency photons escape far away from the ionizing centers and contribute to global heating. This can be simplified when the distance traveled by the photon before being absorbed exceeds the mean distance between sources. As the comoving mean distance between sources is on the order of 1 Mpc at  $z \simeq 20$  for many of the models we consider, it is a good approximation for our study.

In calculating far zone temperature, we essentially take into account all the X-ray frequencies emitted by all the sources since the time they were turned on. To calculate the increase in temperature due to all faraway sources, we choose a random point and calculate the increase in temperature at that point due to sources that lie in a shell of thickness  $dR_0$  at distance  $R_0$  and then we integrate it over all  $R_0$ . We can take the upper limit of  $R_0$  to correspond the redshift of star formation  $R_{\text{final}} = R_0(z_{\star})$ . If we take the minimum value of  $R_0$  to be 0, we get the total (average) temperature increase due to all sources over the history of the universe.

Using the global ionization fraction for the redshift of the chosen shell  $f_i(z(R_0))$ , the volume of ionized gas inside this shell at comoving distance  $R_0$  is,  $4\pi R_0^2 dR_0 f_i(z(R_0))$ . Therefore, we can compute the impact of distant sources by replacing  $4\pi/3 R_x^3$  in Eq. (16) with  $4\pi R_0^2 dR_0 f_i(z(R_0))$  and integrate over  $R_0$ . This gives us:

$$\begin{aligned}\Delta T'_{\text{bg}} &= \frac{h f_H \alpha N_{\text{heat}} f_{\star} n_0 \nu_{\min}^{\alpha}}{k_B \zeta} (1 + z'_0)^2 \int_0^{R_0(z_{\star})} dR_0 \int_{t(z_{\star})}^{t(z)} dt' \frac{\dot{f}_{\text{coll,g}}(t')}{f_{\text{coll,g}}(t')} f_i(t') \left( \frac{1 + z'}{1 + z} \right)^{\alpha+1} \\ &\quad \int_{\nu'_{\min}}^{\infty} d\nu' \nu'^{-\alpha-4} e^{-\tau(R_0, \nu')} \sum_i (\nu' - \nu_i) x_i \sigma_{i0} \nu_i^3\end{aligned}\tag{17}$$

### 2.2.3. Overlap

During the initial phase of the evolution of the heated bubbles, when the ionized and partially heated fractions ( $f_i$  and  $f_h$ , respectively) are small, the partially heated fraction grows and so does the background temperature. At low redshift, the heating bubbles will expand and start to overlap. In this sub-section, we discuss how we take into account the impact of these overlaps. Defining the ionization volume fraction:

$$f_i = \sum_{R_x} \frac{4\pi}{3} N(R_x) R_x^3\tag{18}$$

where,  $R_x$  are radii of ionization bubbles and  $N(R_x)$  is the number density of bubbles with ionization radius  $R_x$ . Similarly, we can define the volume fraction due to heating bubbles to be,

$$f_{hb} = \sum_{R_x} \frac{4\pi}{3} N(R_x) (R_h^3 - R_x^3) \quad (19)$$

This quantity can exceed unity due to significant overlaps as the universe evolves. Therefore, we define another quantity  $f_h$ , that corresponds to the actual volume fraction occupied by heating bubbles. This can be derived by recognizing that, in the case of overlap, within every heating bubble, there can be part of another heating bubble or ionization bubble:

$$\begin{aligned} f_h &= \sum_{R_x} \frac{4\pi}{3} N(R_x) (R_h^3 - R_x^3) (1 - f_i - f_h) \\ &= f_{hb} (1 - f_i - f_h) \end{aligned}$$

This gives us,

$$f_h = \frac{f_{hb}(1 - f_i)}{1 + f_{hb}}$$

$f_h$  remains less than unity even if the value of  $f_{hb}$  becomes much larger than unity and approaches  $f_{hb}$  when the heating and ionization fractions are small. This allows us to successfully model overlap of heating bubbles.

Also, since bubbles overlap, the temperature of a profile around an ionizing source should contain contribution due to other overlapping bubbles.

$$T_p = T_s + T_o \quad (20)$$

Here  $T_p$ , the resultant temperature, is the sum of  $T_s$ , the temperature due a nearby source and  $T_o$ , the average contribution due to overlaps. We recursively define  $T_o$  as,

$$\begin{aligned} T_o &= \sum_{R_x} \sum_s f_s (T_s + T_o) \\ &= \sum_{R_x} \sum_s \frac{4\pi}{3} N(R_x) \frac{f_h}{f_{hb}} ((R_s + \Delta R_s)^3 - R_s^3) T_s + f_h T_o \\ &= \frac{1}{1 - f_h} \sum_{R_x} \sum_s \frac{4\pi}{3} N(R_x) \frac{f_h}{f_{hb}} ((R_s + \Delta R_s)^3 - R_s^3) T_s \end{aligned} \quad (21)$$

For notations, please refer to section 3.2. We add  $T_o$  to the fluctuations, but subtract  $T_o/f_n$  from background to maintain the energy budget.

#### 2.2.4. Modelling

Eqs. (16) and (17) can be used to compute the temperature profile for a single self-ionized region and the evolution of global heating.

We use the following prescription for defining the near- and far-zones. The radius of the near zone is defined as the distance at which the temperature increase due to that source (over its history) is less than 1 K. The temperature in the far zone depends on the choice of minimum  $R_0$  in Eq. (17). We choose  $R_0 = 0$  which means the photon energy absorbed in the near zone is also included. However, as we can independently estimate the total amount of energy absorbed in the near zone, we subtract this energy from the energy budget used to estimate the far-zone temperature. The far zone temperature is then added to the temperature profile of the near zone, to consistently take into account the fact that Eq. (17) gives the global temperature at all points including the near zone.

We note that while the definition of the radius of the locally heated region is somewhat arbitrary, its impact on the break up of energy budget is negligible. Also, and importantly, the correlation functions as defined in the next sections are minimally affected by this definition as the correlation functions depend only upon the gradient of temperature.

We explore three parameters to model heating in this paper:

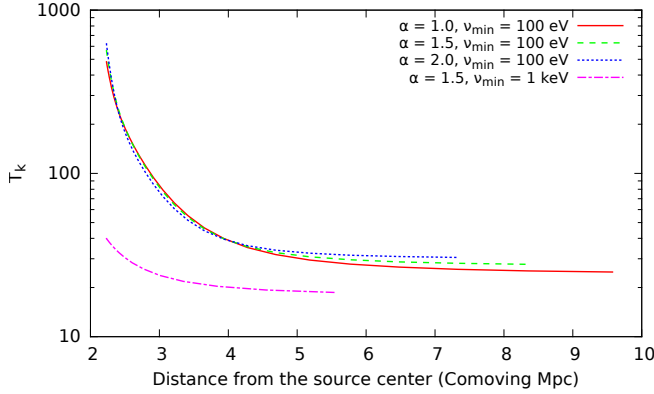


**Figure 3.** Heating profiles around a bubble are shown at  $z = 17$  for various values of  $\alpha$  and  $\nu_{\min}$  with  $\zeta = 10$  and  $N_{\text{heat}} = 1.0$ . It is seen that for  $\nu_{\min} > 1$  keV the temperature is smaller and the profile around a source is shallow or there is less distinction between the near- and far-zone (for details see text).

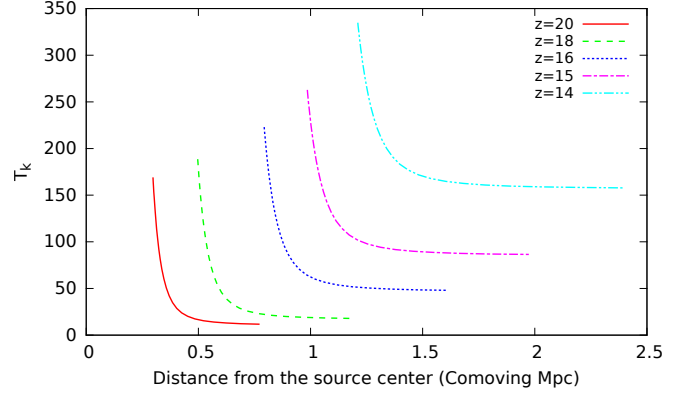


**Figure 4.** Evolution of the heating profile around an ionized bubble is plotted for  $\alpha = 1.5$ ,  $\nu_{\min} = 100$  eV,  $\zeta = 10$ , and  $N_{\text{heat}} = 1.0$ . The size of the fiducial ionized bubble is assumed to grow as the mean ionized fraction in the universe. The smallest radius in each profile displayed is the size of the ionized region. The profiles shown reflect the growth of mean ionization fraction and the increase in background temperature.

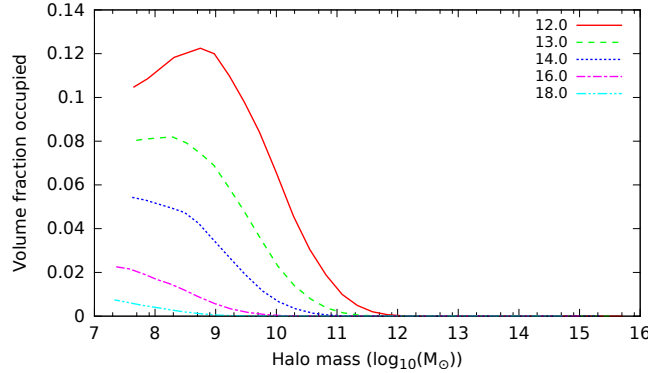


**Figure 5.** The evolution of the size distribution of heated regions (see text for details) as a function of halo mass is shown for  $\zeta = 10$ ,  $\alpha = 1.5$  and  $N_{\text{heat}} = 1$ .

- $\alpha$  = X-ray spectrum power index. We take three possible values, 1.0, 1.5 and 2.0, with the middle value to be standard case. For higher value of  $\alpha$ , there are more photons at low frequency. These photons more effectively heat up the medium since there is higher probability of them being absorbed. Therefore, with higher  $\alpha$ , the background temperature is high and the heating profiles are steeper.
- $N_{\text{heat}}$ : Number of X-ray photons emitted per stellar baryon. For our study, we assume  $N_{\text{heat}}$  in the range: 0.1–10.0.
- $\nu_{\min}$ : Minimum X-ray frequency escaping the source halo. We take two possible values, 100 eV and 1 keV. For a given  $N_{\text{heat}}$ , higher value of  $\nu_{\min}$  means the emitted photons are more energetic. They free stream into the medium and uniformly heat medium with little fluctuations around source halos.

To explore more complicated models where the X-ray luminosity is not power law (e.g. [Fialkov et al. \(2014\)](#)), we can take  $N_{\text{heat}}$  and  $\alpha$  to be a function of frequency  $\nu$  and time. However, we do not explore such models in this paper.

In Figure 3 we plot temperature profiles around an ionization bubble at  $z = 17$  for  $\zeta = 10$ ,  $N_{\text{heat}} = 1.0$ , and three values of  $\alpha$ . The figure also displays a case when  $\nu_{\min} = 1$  keV. In this case, owing to the absence of low energy photons, the near-zone profile around the source is very shallow. Also, as noted above, the heating is suppressed in this case even in the far zone as many high energy photons remain unabsorbed ([Fialkov et al. \(2014\)](#)). In Figure 4

we show the evolution of the heating profile around an ionized bubble (similar results have been obtained by e.g. Venkatesan & Benson (2011); Ghara et al. (2015)). This figure captures the impact of the growth of ionized region and the average ionization fraction on the heating profile and the background temperature. In Figure 5 we show the heating bubble size distribution corresponding to ionization bubbles from Figure 2.

### 2.3. Lyman- $\alpha$ radiation

As noted in section 2, Lyman- $\alpha$  radiation plays an important role in determining the brightness temperature of H I emission from EoR. For EoR studies, all the radiation between Lyman- $\alpha$  and Lyman-limit is referred to as Lyman- $\alpha$  and we shall follow this convention. Photons in this frequency band are not absorbed in the H II region but escape into the surrounding medium and redshift until its frequency nearly equals the resonant frequency of one of the Lyman series lines. Given the complicated frequency structure of Lyman-series lines, these photons are absorbed at varying distances from the source. Our aim here is to determine the conditions under which this radiation couples spin temperature of the H I line  $T_S$  to matter kinetic temperature  $T_K$ . This coupling depends on two factors: the region of influence of the Lyman- $\alpha$  radiation and the coupling coefficient  $y_\alpha$  (Eq. (1)).

First, we find the Lyman- $\alpha$  influence region, which is mainly determined by the distance traveled by the Lyman- $\beta$  photons to redshift to Lyman- $\alpha$  frequency. If these photons were emitted at  $z = z_e$  and absorbed at  $z = z_a$  with  $\nu_e = \nu_\beta$  and  $\nu_a = \nu_\alpha$ , then, the comoving distance traveled by the photon before it is absorbed in an expanding universe is:

$$R_{\max} \simeq \frac{1422 \text{ Mpc}}{(1 + z_e)^{1/2}}$$

We note that  $R_{\max}$  is much larger than the mean distance between ionization bubbles at any redshift. For  $\zeta = 15$ , the values of mean comoving distance between bubbles for redshift 25, 20, 15 is 9.66 Mpc, 2.61 Mpc and 1.08 Mpc respectively. Therefore Lyman- $\alpha$  regions are very large and merge very early. However, this would create homogeneous coupling to H I atoms only if  $y_\alpha$  is high enough (Eq. (1)).

Lyman- $\alpha$  coupling coefficient,  $y_\alpha$  is a function of Lyman- $\alpha$  photon (physical) number density  $n'_\alpha$  (Field (1958); Chen & Miralda-Escudé (2004)):

$$y_\alpha = 5.9 \times 10^{11} \frac{n'_\alpha}{T_K^{3/2}} \quad (22)$$

For efficient coupling between kinetic temperature  $T_K$  and spin temperature  $T_S$  we need  $y_\alpha \gtrsim T_{\text{CMB}}/T_K$ .

We assume that Lyman- $\alpha$  contribution comes through two main factors: Lyman- $\alpha$  emitted from the sources and Lyman- $\alpha$  created due to X-ray photo-electrons (Venkatesan et al. (2001)). The latter is generally negligible. To calculate the number density of Lyman- $\alpha$  photons from ionizing sources, we use the same method applied in the previous section, which seeks to express the Lyman- $\alpha$  photon luminosity in terms of the radii of ionizing regions. This method allows us to compute both the near- and far-zone contribution from Lyman- $\alpha$  photons. In this paper, we compute only the far-zone contribution which comes from photons between Lyman- $\alpha$  and Lyman- $\beta$ . Assuming flat spectrum between Lyman- $\alpha$  and Lyman- $\beta$ , the number density of Lyman- $\alpha$  photons at a comoving distance  $R_0$  from the source is:

$$n'_{\alpha,\star} = \frac{\dot{N}_\alpha}{4\pi c R_0^2} \frac{2\Delta\nu_\alpha}{\nu_\beta - \nu_\alpha} \frac{(1 + z')^3}{1 + z}$$

Here  $\dot{N}_\alpha$  is the Lyman- $\alpha$  luminosity of a given halo.  $\Delta\nu_\alpha = \sqrt{8kT \ln(2)/m_p c^2} \nu_\alpha$  is the Doppler line width and this factor arises because at the source the photons are emitted with frequencies between  $\nu_\beta$  and  $\nu_\alpha$ , but the only frequencies which are absorbed at redshift  $z'$  are in the range of  $\Delta\nu_\alpha$  around  $\nu_\alpha$ .

The Lyman- $\alpha$  luminosity,  $\dot{N}_\alpha$ , can be expressed in terms of the size of ionization halo assuming that the Lyman- $\alpha$  luminosity scales with ionizing luminosity with a factor  $f_L$  and the balance between ionization and recombination in the ionizing region:

$$\dot{N}_\alpha = f_L \frac{4\pi}{3} n_0^2 \alpha_B C R_x^3 (1 + z)^3$$

Here  $10 < f_L < 100$  (e.g. Chen & Miralda-Escudé (2004)).

We can calculate the Lyman- $\alpha$  number density due to faraway sources in the same way as described in the previous section. In thin shell of width  $dR_0$  at comoving distance  $R_0$  from the receiving point, the contributing ionization fraction is,  $4\pi R_0^2 dR_0 f_i(z)$ . Therefore we integrate over  $R_0$ . Here we take the lower limit of the integral  $R_0 = 0$  while the upper limit is given by the Lyman- $\alpha$  influence region.

$$\begin{aligned} n'_{\alpha, \text{bg}} &= \frac{f_L n_0^2 \alpha_B C}{c} \int_0^{R_{\text{max}}} dR_0 f_i(z) \frac{2\Delta\nu_\alpha}{\nu_\beta - \nu_\alpha} (1+z')^3 (1+z)^2 \\ &= 4.71 \frac{f_L n_0^2 \alpha_B C}{c^2} \sqrt{\frac{k}{m_p}} \frac{\nu_\alpha}{\nu_\beta - \nu_\alpha} (1+z')^3 \int_0^{R_{\text{max}}} dR_0 f_i(z) T_K(z)^{1/2} (1+z)^2 \end{aligned} \quad (23)$$

Here  $R_{\text{max}}$  is distance corresponding to  $z_{\text{max}} = (1+z')(\nu_\beta/\nu_\alpha) - 1$ .

From Eq. (1) it follows that for  $q \equiv y_\alpha T_K / T_{\text{CMB}} \geq 1$  we expect the spin temperature to relax to the matter temperature  $T_K$ . Using Eqs. (22) and (23) we can compute  $y_\alpha$ . Given the complicated temperature structure of the regions outside the ionized region,  $q$  can vary substantially as it scales as  $T_K^{-1/2}$ . We find that for all the models we consider here,  $q$  exceeds unity for  $z < 20$ , e.g. for  $\zeta = 10$ ,  $\alpha = 1.5$ ,  $N_{\text{heat}} = 0.5$ ,  $f_L = 100$ ,  $C = 2$  and  $z = 20$ , the background temperature is 9.1 K, the value of  $y_\alpha$  is 40 and  $q = 6.3$ .

Here we do not calculate the effect of higher order Lyman transitions (eg. from Lyman- $\gamma$  to Lyman- $\beta$ ), since their total number density is less than photons between Lyman- $\beta$  and Lyman- $\alpha$ . Moreover, they will be absorbed closer to the source.

### 3. AUTO-CORRELATION OF BRIGHTNESS TEMPERATURE $T_B$

The auto-correlation of  $\psi$  (Eq. (3)) can be defined as:

$$\begin{aligned} \mu &= \langle \psi_1 \psi_2 \rangle - \langle \psi \rangle^2 \\ &= \langle n_1(1+\delta_1)(1-s_1)n_2(1+\delta_2)(1-s_2) \rangle - \langle n_1(1+\delta_1)(1-s_1) \rangle^2 \end{aligned} \quad (24)$$

Here,  $n_1$ ,  $\delta_1$  and  $s_1$  are values of ionization, overdensity and heating ( $T_{\text{CMB}}/T_S$ ) at point 1 ( $\mathbf{r}_1$ ). Similarly,  $n_2$ ,  $\delta_2$  and  $s_2$  are values at point 2 ( $\mathbf{r}_2$ ). It should be noted that the autocorrelation function  $\mu$  is function of  $r = |\mathbf{r}_2 - \mathbf{r}_1|$  as the process of reionization is statistically homogeneous and isotropic. To calculate  $\mu$ , we need to find all the pairs of points which are separated by a distance  $r$ , and average them over the entire space. To compute the correlation function we use geometric arguments to find the probability of pairs with given values and take their weighed average.

Eq. (24) can be greatly simplified if we assume that density has no correlation with ionization or heating ( $\eta = \langle n\delta \rangle = 0$  and  $\langle s\delta \rangle = 0$ )<sup>2</sup>. This gives us:

$$\langle n_1 n_2 (1 + \delta_1 + \delta_2 + \delta_1 \delta_2) (1 - s_1 - s_2 + s_1 s_2) \rangle = (1 + \xi) \langle n_1 n_2 (1 - s_1 - s_2 + s_1 s_2) \rangle$$

Where  $\xi = \langle \delta(\mathbf{r}_1) \delta(\mathbf{r}_2) \rangle$  is the auto-correlation function of the H I density perturbation; we compute  $\xi$  using the  $\Lambda$ CDM model power spectrum, assuming the relative bias between the dark matter and the H I,  $b = 1$ . And,

$$\begin{aligned} \langle n_1(1+\delta_1)(1-s_1) \rangle &= \langle 1+\delta_1 \rangle \langle n_1(1-s_1) \rangle \\ &= f_n - \langle n_1 s_1 \rangle \end{aligned}$$

Since  $\langle \delta \rangle = 0$  and  $f_n = \langle n \rangle$  is defined as the dimensionless average neutral volume fraction at that redshift. This finally yields:

$$\mu = (1 + \xi) (\langle n_1 n_2 \rangle - \langle n_1 n_2 s_1 \rangle - \langle n_1 n_2 s_2 \rangle + \langle n_1 n_2 s_1 s_2 \rangle) - (f_n - \langle n_1 s_1 \rangle)^2$$

We can greatly simplify correlation functions higher than second order. Let us first consider  $\langle n_1 n_2 s_1 \rangle$ . This corresponds to the joint probability that the point  $\mathbf{r} = \mathbf{r}_1$  is both neutral and heated to a temperature such that  $s = s_1$  while the second point is neutral. As noted above,  $n$  can be either unity (neutral point) or zero (ionized point) while  $s$  can take any arbitrary value depending on the kinetic temperature. However, in our model  $T_K \gg T_{\text{CMB}}$  if and only if that

<sup>2</sup> We make this assumption in the paper. These cross-correlations can be computed using excursion set formalism, e.g. [Furlanetto et al. \(2004a\)](#) for density-ionization cross-correlation, which is generally sub-dominant to other terms we retain.

point is ionized ( $T_K \sim 10^4$  K). In other words, for a point  $s = 0$  if and only if that point has  $n = 0$ . Therefore the condition of point 1 being neutral ( $n_1 = 1$ ) is fulfilled by it being not heated to very high temperature ( $s_1 \neq 0$ ). This allows us to simplify higher point correlation functions as:

$$\begin{aligned}\langle n_1 n_2 s_1 \rangle &= \langle n_2 s_1 \rangle \\ \langle n_1 n_2 s_2 \rangle &= \langle n_1 s_2 \rangle \\ \langle n_1 n_2 s_1 s_2 \rangle &= \langle s_1 s_2 \rangle\end{aligned}$$

And since we choose two points randomly, we also have,

$$\langle n_1 s_2 \rangle = \langle n_2 s_1 \rangle$$

Finally, we have,

$$\mu = (1 + \xi)(\langle n_1 n_2 \rangle - 2\langle n_1 s_2 \rangle + \langle s_1 s_2 \rangle) - (f_n - \langle n_1 s_1 \rangle)^2 \quad (25)$$

Here we have introduced cross-correlations between kinetic temperature (heating) and ionization ( $\langle n_1 s_2 \rangle$ ) and auto-correlation of heating ( $\langle s_1 s_2 \rangle$ ). These terms have significant effect in brightness temperature correlation. As noted above, all the 2-point correlations are function of distance between two points  $|\mathbf{r}_2 - \mathbf{r}_1|$ .

In following subsections we explore certain simplifying cases and limits.

### 3.1. Simplifying Cases

#### 3.1.1. Uniform Heating

As a simplifying case, we examine a model where there is uniform heating outside ionized bubbles and all the neutral gas of the IGM is at uniform temperature of  $T_{\text{bg}}$ .

$$\psi = n(1 + \delta)(1 - s_b)$$

The correlation is,

$$\begin{aligned}\mu &= (1 - s_b)^2 \langle n_1(1 + \delta_1)n_2(1 + \delta_2) \rangle - (1 - s_b)^2 \langle n_1(1 + \delta_1) \rangle^2 \\ &= (1 - s_b)^2 ((1 + \xi)\langle n_1 n_2 \rangle - f_n^2)\end{aligned} \quad (26)$$

Here  $s_b = T_{\text{CMB}}/T_{\text{bg}}$ . At early times,  $T_{\text{bg}}$  can approach the adiabatically cooled temperature of the IGM gas which is smaller than  $T_{\text{CMB}}$ . If ionization fraction is too small,  $\langle n_1 n_2 \rangle \simeq f_n^2 \simeq 1$ . This gives us,

$$\mu = \xi(1 - s_b)^2$$

At late times  $T_{\text{bg}} \gg T_{\text{CMB}}$  owing to X-ray heating, driving  $s_b$  to zero. Which gives,

$$\mu = -f_n^2 + (1 + \xi)\langle n_1 n_2 \rangle \quad (27)$$

This result is consistent with [Zaldarriaga et al. \(2004\)](#).

#### 3.1.2. Correlation at Very Large and Small Scales

We can compute the small and large scale limits of the correlation function given by Eq. (25) under fairly general conditions. Both ionization and heating inhomogeneities are caused by bubbles of a given size distribution, which determine the scales of correlation. As discussed in the foregoing, the size distribution evolves and bubbles could have complicated profiles. However, for scales greater than the largest bubbles, the correlation function owing the ionization and heating inhomogeneities vanish, and the H I correlation function is determined by only density perturbations. In this limits we get:

$$\begin{aligned}\langle n_1 n_2 \rangle &= \langle n_1 \rangle \langle n_2 \rangle = f_n^2 \\ \langle n_1 s_2 \rangle &= \langle n_1 \rangle \langle s_2 \rangle = f_n \langle s \rangle \\ \langle s_1 s_2 \rangle &= \langle s_1 \rangle \langle s_2 \rangle = \langle s \rangle^2\end{aligned}$$

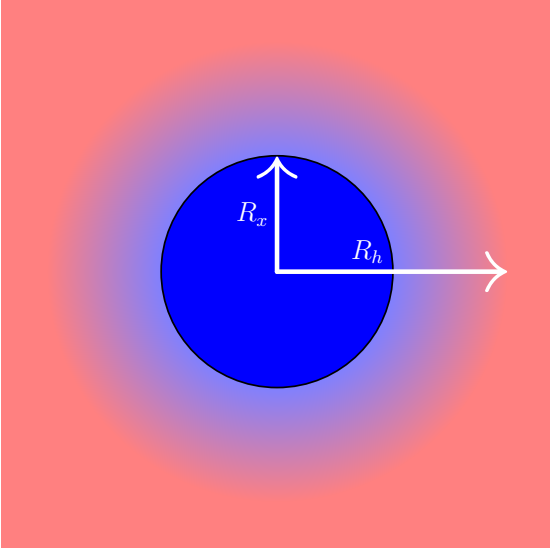


**Figure 6.** The topology of the ionized and the heated region typical of partially heated universe is shown. The ionized region of size  $R_x$  (with sharp boundary) is seen to be surrounded by a heated fuzzy region of radius  $R_h$ . The colour scheme shows the temperature,  $T$ .  $T \simeq 10^4$  in the ionized regions and it is much smaller in the heated region. It falls as distance from the source center and smoothly merges with the background.

Therefore,

$$\begin{aligned}\mu &= (1 + \xi)(\langle n_1 n_2 \rangle - 2\langle n_1 s_2 \rangle + \langle s_1 s_2 \rangle) - (f_n - \langle n_1 s_1 \rangle)^2 \\ &= (1 + \xi)(f_n - \langle s \rangle)^2 - (f_n - \langle s \rangle)^2 \\ &= \xi(f_n - \langle s \rangle)^2\end{aligned}\tag{28}$$

In this limit, the correlation function scales as the density correlation function  $\xi$ . We also note that the correlation function vanishes when  $f_n = \langle s \rangle$  (close to global heating transition).

In the small scale limit ( $\mathbf{r}_2 = \mathbf{r}_1$ ), we get:

$$\begin{aligned}\mu &= (1 + \xi_0)(\langle n_1 n_1 \rangle - 2\langle n_1 s_1 \rangle + \langle s_1 s_1 \rangle) - (f_n - \langle n_1 s_1 \rangle)^2 \\ &= (1 + \xi_0)(f_n - 2\langle s \rangle + \langle s^2 \rangle) - (f_n^2 - 2f_n \langle s \rangle + \langle s \rangle^2)\end{aligned}\tag{29}$$

Here  $\xi_0 = \xi(0)$  or the correlation function computed at zero lag which equals RMS of density perturbations. Since Eq. (29) gives an RMS, it is always positive.

We verify Eqs. (28) and (29) as the large and small scale limits of the H I correlation function computed using methods described in the next sections.

### 3.2. Modelling and Notations

Our aim in this paper is to analytically model the early phase of EoR. This issue can essentially be reduced to computing the auto-correlation of neutral fraction  $\langle n_1 n_2 \rangle$ , the ionization-heating cross-correlation  $\langle s_1 n_2 \rangle$ , and the heating auto-correlation function  $\langle s_1 s_2 \rangle$ . We make several assumptions to make this problem analytically tractable. The main assumption is that for a given self-ionized region the heating and ionization bubbles are spherical and concentric and the ionization centers are uncorrelated. Each self-ionized and heating region can be treated as isolated so long as both the ionization and heating fractions are small, which is expected during the early phase of reionization. As discussed in section 2.2, X-ray heating can be split into near- and far-zone effects. While the near-zone effects are owing to the vicinity of a self-ionized region, the far-zone effects take into account the impact of all the sources and their evolution. We model them both in this paper. An additional complication in the case of heating is that

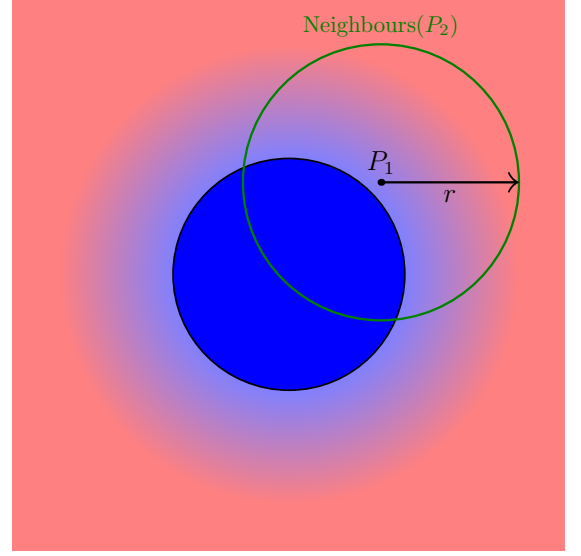


**Figure 7.** Randomly choosing a point and finding correlation with its neighbour at distance  $r$

near-zone heating have a smooth profile around them, as opposed to ionized bubbles which have uniform ionization within the bubble with a sharp boundary. We explicitly account for the heating rate as a function of distance from the source and its smooth merger into the background. In Figure 6 we show the geometry of the self-ionized region and the heating zone beyond it. To compute correlations we assume two random points separated by a distance  $r$  as shown in Figure 7. The formalism used for the computation of correlation functions is described in the Appendix.

We assume that at a given  $z$ , the ionized bubbles have various radii  $R_x$ . The number density of bubbles of radius  $R_x$  is  $N(R_x)$ . Between  $R_x$  and  $R_h$ , the outer boundary of heating bubble (Figure 6), we take shells of thickness  $\Delta R(R_x, s)$ , having nonzero temperature  $s = T_{\text{CMB}}/T_S$ . A detailed description of notations followed in this paper is as follows:

- $R_{xa}$  = Radius of ionization bubble  $a$ . When there is no confusion regarding the bubble in question, we drop the subscript  $a$ .
- $R_{ha}$  = Outer radius of the heating bubble of the given source  $a$ .  $R_h = R_h(R_x)$
- $P(\widetilde{n_p}(R_x)) = P(\widetilde{n_p} \subset R_x)$  = Probability that point  $p$  belongs to an ionization bubble of radius  $R_x$ . If it is randomly chosen,

$$P(\widetilde{n_p}(R_x)) = N(R_x) \frac{4\pi}{3} R_x^3$$

- $P(\widetilde{n_p})$  = Probability of point  $p$  being ionized.  $P(\widetilde{n_p}) = f_i$  = Average ionized volume fraction if point  $p$  is randomly chosen.

$$f_i = \sum_{R_x} P(\widetilde{n_p}(R_x)) = \sum_{R_x} N(R_x) \frac{4\pi}{3} R_x^3$$

- $P(n_p)$  = Probability of point  $p$  being neutral.  $P(n_p) = f_n = (1 - f_i)$  = Average neutral volume fraction if point  $p$  is randomly chosen.

$$f_n = 1 - \sum_{R_x} N(R_x) \frac{4\pi}{3} R_x^3$$

- Total volume fraction due to heating bubbles (without taking into account the overlaps),

$$f_{hb} = \sum_{R_x} N(R_x) \frac{4\pi}{3} (R_h^3 - R_x^3) \quad (30)$$

This quantity can be larger than unity.

- $f_h$  = Average heated volume fraction if the point is randomly chosen = Volume fraction occupied by heating bubbles after taking into account the overlaps.

$$\begin{aligned} f_h &= \sum_{R_x} N(R_x) \frac{4\pi}{3} (1 - f_i - f_h)(R_h^3 - R_x^3) \\ &= \frac{f_{hb}(1 - f_i)}{1 + f_{hb}} \end{aligned} \quad (31)$$

- $P(s_b) = f_b$  = Average background volume fraction if the point is randomly chosen.

$$\begin{aligned} f_b &= 1 - f_i - f_h \\ &= \frac{1 - f_i}{1 + f_{hb}} \end{aligned} \quad (32)$$

This also gives,

$$f_h = f_{hb} f_b \quad (33)$$

It should be noted that when  $f_{hb}$  is small,  $f_h$  approaches  $f_{hb}$  and  $f_b \simeq 1 - f_i - f_{hb}$ , the values expected if the overlap is neglected.

- $R_{a,s} = R(s, R_{xa})$  = Inner radius of the shell with temperature  $s$  in the heating bubble corresponding to ionization radius  $R_{xa}$ . We simplify it to  $R_s$  when there is no ambiguity about the value of  $R_{xa}$ .
- $\Delta R_{a,s} = \Delta R(s, R_{xa})$  = Thickness of shell with temperature  $s$  in the heating bubble corresponding to ionization radius  $R_{xa}$ . We simplify it to  $\Delta R_s$  when there is no ambiguity about the value of  $R_{xa}$ .
- $P(s, R_x)$  = Probability that the chosen point has temperature  $s$  and lies in bubble with ionization radius  $R_x$ .

$$\begin{aligned} P(s, R_x) &= N(R_x) \frac{4\pi}{3} \frac{f_h}{f_{hb}} ((R_s + \Delta R_s)^3 - R_s^3) \\ &= N(R_x) \frac{4\pi}{3} f_b ((R_s + \Delta R_s)^3 - R_s^3) \end{aligned}$$

- $P(s)$  = Probability that the randomly chosen point has temperature  $s$ , where  $0 < s < s_b$ .

$$P(s) = \sum_{R_x} P(s, R_x)$$

This also gives,

$$\begin{aligned} f_h &= \sum_s \sum_{R_x} P(s, R_x) \\ &= \sum_{R_x} N(R_x) \frac{4\pi}{3} f_b (R_h^3 - R_x^3) \end{aligned}$$

And,

$$\begin{aligned} f_b &= 1 - \sum_{R_x} \sum_s P(s, R_x) - \sum_{R_x} P(\tilde{n}(R_x)) \\ &= 1 - \sum_{R_x} N(R_x) \frac{4\pi}{3} (f_b (R_h^3 - R_x^3) + R_x^3) \end{aligned}$$

- $P(n_p \cap n_q)$  = Probability that from two chosen points  $p$  and  $q$ , both are neutral.
- $P(n_p \cap s_b)$  = Probability of point  $p$  being neutral and point  $q$  being in background (outside any heating bubble).
- $P(s_b \cap s_b)$  = Probability that both points are in background.
- $P(s_b \cap s_q)$  = Probability point  $p$  is background and point  $q$  is partially heated with temperature  $s$ .
- $P(s_p \cap s_q)$  = Probability that both points are partially heated with temperature  $s_p$  and  $s_q$  respectively.

### 3.3. Complete Model

Our main aim is to calculate ionization and heating correlations for epochs at which ionization volume fraction is small. This ensures that ionization bubbles are separate and non-overlapping. However, as described in section 2.2, our formulation allows us to deal with overlap of heating bubbles. We describe in detail our formalism to compute the neutral fraction auto-correlation, neutral fraction-heating cross-correlation and heating auto-correlation next.

#### 3.3.1. Correlation of Neutral Region ( $\langle n_1 n_2 \rangle$ )

We need to find the probability (fraction) of pairs with both points neutral (outside the ionization bubble).

$$\begin{aligned} \langle n_1 n_2 \rangle &= 1^2 P(n_1 \cap n_2) + 0 P(n_1 \cap \tilde{n}_2) + 0 P(\tilde{n}_1 \cap n_2) + 0 P(\tilde{n}_1 \cap \tilde{n}_2) \\ &= P(n_1 \cap n_2) \end{aligned}$$

Using Eqs. (A3),

$$P(n_1 \cap n_2) = P(n_1) - P(n_1 \cap \tilde{n}_2)$$

First, we assume that point 2 is ionized. Therefore it lies in *some* ionized bubble. The statement that its neighbor (point 1) at distance  $r$  lies in a neutral region means that point 1 lies outside *that* bubble and it lies outside *any other* bubble. Using Eq. (A2),

$$\begin{aligned} P(n_1 \cap \widetilde{n}_2) &= P((n_1(\text{out same}) \cap n_1(\text{out other})) \cap \widetilde{n}_2) \\ &= P(n_1(\text{out other}) | (n_1(\text{out same}) \cap \widetilde{n}_2)) P(n_1(\text{out same}) \cap \widetilde{n}_2) \end{aligned}$$

If we assume that the bubbles are uncorrelated and non-overlapping then  $P(n_1(\text{out other}) | (n_1(\text{out same}) \cap \widetilde{n}_2))$  is the probability that point 1 is neutral given that point 2 lies in *some* bubble and point 1 lies outside *that* bubble. This quantity is equal to average neutral fraction  $f_n$  in the present case.<sup>3</sup>

Now, we need to find  $P(n_1(\text{out same}) \cap \widetilde{n}_2)$  = Probability that point 2 is in an ionization bubble and point 1 lies out of that bubble. Point 2 can be in bubble with any radius  $R_x$ . Therefore,

$$\begin{aligned} P(n_1(\text{out same}) \cap \widetilde{n}_2) &= \sum_{R_x} P(n_1(\text{out same}) \cap \widetilde{n}_2(R_x)) \\ &= \sum_{R_x} P(\widetilde{n}_2(R_x)) P(n_1(\text{out same}) | \widetilde{n}_2(R_x)) \\ &= \sum_{R_x} N(R_x) \frac{4\pi}{3} R_x^3 D(x, R_x) \end{aligned}$$

Where  $P(n_1(\text{out same}) | \widetilde{n}_2(R_x)) = D(x, R_x)$  = Probability that point 1 is out of the bubble given that point 2 is inside bubble of some radius  $R_x$ . Therefore,

$$\langle n_1 n_2 \rangle = f_n - f_n \sum_{R_x} N(R_x) \frac{4\pi}{3} R_x^3 D(r, R_x) \quad (34)$$

This result is derived and explored in [Zaldarriaga et al. \(2004\)](#). It also follows from our discussion that the scenario envisaged in Figure 6 is valid at early time.

### 3.3.2. Correlation between Neutral region and Heating ( $\langle n_1 s_2 \rangle$ )

We need to find the correlation between neutral points and points with  $s \neq 0$ .

$$\langle n_1 s_2 \rangle = s_b P(n_1 \cap s_b) + \sum_{0 < s < s_b} s P(n_1 \cap s) \quad (35)$$

Here  $s_b$  corresponds to the background (far zone) temperature at any redshift. The first term can be written as:

$$P(n_1 \cap s_b) = P(s_b) - P(s_b \cap \widetilde{n}_1)$$

We apply the procedure followed in the previous section. As point 1 is ionized, it lies in some ionization bubble. The statement that its neighbor (point 2) at distance  $r$  lies in background region means that point 2 lies outside the heating bubble corresponding to that ionization bubble and it lies outside any other heating bubble.

$$P(s_b \cap \widetilde{n}_1) = P(s_2(\text{out other}) | (s_2(\text{out same}) \cap \widetilde{n}_1)) P(s_2(\text{out same}) \cap \widetilde{n}_1)$$

As the bubbles are assumed to be non-overlapping and uncorrelated  $P(s_b(\text{out other}) | (s_b(\text{out same}) \cap \widetilde{n}_1))$  gives the probability that point 2 is in background region given that point 1 lies in some ionization bubble and point 2 lies outside heating bubble corresponding to that ionization bubble. This probability equals the fraction of universe heated at background temperature,  $f_b$ <sup>4</sup>.

<sup>3</sup> If we assume that bubbles are uncorrelated and randomly distributed, then once a point is outside a certain bubble, its probability to be ionized or neutral is proportional to global ionized or neutral fractions respectively. However, this formalism applies because we are assuming infinite volume. If we had assumed finite volume (as would be the case for a simulation), the ionized volume fraction around an ionized bubble will be less than the global ionized volume fraction since we need to take into account the volume occupied by the said ionization bubble. For a finite volume, this effect should cause anti-correlation between bubbles. Throughout this paper, we assume infinite volume for averaging.

<sup>4</sup> Refer to footnote 3.

Our next task is to compute  $P(s_2(\text{out same}) \cap \widetilde{n}_1)$  which is the probability of point 1 being in an ionization bubble and point 2 being out of the heating bubble corresponding to that ionization bubble. Given the distribution of radii of ionization bubbles,  $R_x$ , we have,

$$P(s_2(\text{out same}) \cap \widetilde{n}_1) = \sum_{R_x} N(R_x) \frac{4\pi}{3} R_x^3 P(s_2(\text{out same}) | \widetilde{n}_1(R_x))$$

We see that  $P(s_2(\text{out same}) | \widetilde{n}_1(R_x)) = E(r, R_x, R_h(R_x))$ , the probability that point 2 is out of the heating bubble corresponding to the ionization bubble of radius  $R_x$  in which point 1 lies. Thus we have:

$$P(n_1 \cap s_b) = f_b - f_b \sum_{R_x} N(R_x) \frac{4\pi}{3} R_x^3 E(r, R_x, R_h(R_x)) \quad (36)$$

We also note that, in the limit  $R_h \rightarrow R_x$ ,  $E(r, R_x, R_h) \rightarrow D(r, R_x)$  which allows us to take the limit in which the region outside the ionizing bubbles is uniformly heated.

Now, we need to find  $P(n_1 \cap s)$ , where  $0 < s < s_b$ . Here, point 2 is inside a heating bubble, but outside ionization bubble. Point 2 can be in heating bubble of any radius, thus,

$$P(n_1 \cap s) = \sum_{R_x} P(s, R_x) P(n_1 | s(R_x))$$

Where  $P(n_1 | s(R_x))$  is the probability that point 1 is in some neutral region given that point 2 is in the partially heated region of ionization bubble of size  $R_x$  with  $s_2 = s$ . If it is outside *that* ionization bubble, then its probability to be neutral = (1 - probability of there being an ionization bubble there). Using result of section 3.3.1,

$$P(n_1 | s(R_x)) = \left( 1 - \sum_{R'_x} N(R'_x) \frac{4\pi}{3} R'_x{}^3 D(r, R'_x) \right) C(r, R_s, R_s + \Delta R_s, R_x)$$

Where  $C(r, P, Q, R)$ , as discussed in Appendix, gives the probability that if point 1 is between radii  $P$  and  $Q$  from the center of a sphere, then its neighbour point 2 at distance  $r$  is outside radius  $R$  of the same sphere. Therefore,

$$P(n_1 \cap s) = \sum_{R_x} N(R_x) \frac{4\pi}{3} f_b ((R_s + \Delta R_s)^3 - R_s^3) \left( 1 - \sum_{R'_x} N(R'_x) \frac{4\pi}{3} R'_x{}^3 D(r, R'_x) \right) C(r, R_s, R_s + \Delta R_s, R_x) \quad (37)$$

This gives us the final expression:

$$\begin{aligned} \langle n_1 s_2 \rangle &= s_b f_b - s_b f_b \sum_{R_x} N(R_x) \frac{4\pi}{3} R_x^3 E(r, R_x, R_h) \\ &+ \left( 1 - \sum_{R'_x} N(R'_x) \frac{4\pi}{3} R'_x{}^3 D(r, R'_x) \right) f_b \sum_{R_x} N(R_x) \frac{4\pi}{3} \sum_{s(R_x)} s ((R_s + \Delta R_s)^3 - R_s^3) C(r, R_s, R_s + \Delta R_s, R_x) \end{aligned} \quad (38)$$

In writing Eq. (38) we have suppressed the dependence of  $R_h$  and  $R_s$  on  $R_x$ .

We also need to calculate correlation between ionization and heating at the same point ( $\langle n_1 s_1 \rangle = \langle s \rangle$ ). The signal will be non-zero only if the chosen point is neutral. Therefore,

$$\langle n_1 s_1 \rangle = s_b f_b + f_b \sum_{R_x} N(R_x) \frac{4\pi}{3} \sum_{s(R_x)} s ((R_s + \Delta R_s)^3 - R_s^3) \quad (39)$$

This quantity can also be represented as the global average of  $s$ , as  $s = 0$  where  $n = 0$ .

### 3.3.3. Correlation of Heating ( $\langle s_1 s_2 \rangle$ )

The signal will be non-zero only if neither of the points are completely heated or, equivalently, both the points lie outside ionized regions. Therefore,  $s_1 \neq 0$  and  $s_2 \neq 0$ .

$$\begin{aligned} \langle s_1 s_2 \rangle &= s_b^2 P((s_1 = s_b) \cap (s_2 = s_b)) + 2s_b \sum_{0 < s < s_b} s P((s_1 = s_b) \cap (s_2 = s)) \\ &+ \sum_{0 < s_p < s_b} \sum_{0 < s_q < s_b} s_p s_q P((s_1 = s_p) \cap (s_2 = s_q)) \end{aligned} \quad (40)$$

Following the logic of sections-3.3.1,

$$P((s_1 = s_b) \cap (s_2 = s_b)) = P(s_b) - P((s_1 = s_b) \cap (s_2 = \tilde{s}_b))$$

If point 2 is not in background region, it can be in ionized or heated profile region. In any case, its neighbour point 1 will be in background region only if it is outside the heated region of the bubble in which point 2 is. Therefore,

$$P((s_1 = s_b) \cap (s_2 = s_b)) = f_b - f_b \sum_{R_x} N(R_x) \frac{4\pi}{3} ((R_h^3 - R_x^3) f_b C(r, R_x, R_h, R_h) + R_x^3 E(r, R_x, R_h)) \quad (41)$$

We have,

$$P((s_1 = s_b) \cap (s_2 = s)) = P(s_1(\text{out other})|(s_1(\text{out same}) \cap (s_2 = s))) P(s_1(\text{out same}) \cap (s_2 = s))$$

Where  $P(s_1(\text{out other})|(s_1(\text{out same}) \cap (s_2 = s)))$  is the probability that point 1 is in background region given that point 2 is partially heated with temperature  $s$  and point 1 is not inside the bubble in which point 2 is. This probability equals the fraction of the universe heated to background temperature,  $f_b$ <sup>5</sup>.  $P(s_1(\text{out same}) \cap (s_2 = s))$  is the probability that point 1 is out of the bubble in which point 2 is, and point 2 is partially heated with temperature  $s$ . As point 2 can be in bubble with any ionization radius  $R_x$ , we have,

$$P(s_1(\text{out same}) \cap (s_2 = s)) = \sum_{R_x} N(R_x) \frac{4\pi}{3} f_b ((R_s + \Delta R_s)^3 - R_s^3) P(s_1(\text{out same})|(s_2 = s)(R_x))$$

$P(s_1(\text{out same})|(s_2 = s)(R_x))$  is the probability that point 1 is out of the bubble which has ionization radius  $R_x$  and which contains point 2 with temperature  $s$ . This equals the probability that point 1 is out of the bubble with outer radius  $R_h$  in which point 2 is located between radius  $R_s$  and  $R_s + \Delta R_s$ . This gives us:

$$P((s_1 = s_b) \cap (s_2 = s)) = f_b \sum_{R_x} N(R_x) \frac{4\pi}{3} f_b ((R_s + \Delta R_s)^3 - R_s^3) C(r, R_s, R_s + \Delta R_s, R_h) \quad (42)$$

In the case where both points are partially heated, these points can belong to the same bubble or they can belong to different bubbles, which gives:

$$P(s_1 \cap s_2) = P(s_1 \cap s_2(\text{same})) + P(s_1 \cap s_2(\text{diff})) \quad (43)$$

Here  $P(s_1 \cap s_2(\text{same}))$  is the probability that points 1 and 2 have temperature  $s_1$  and  $s_2$  respectively and they belong to the same bubble. We calculate  $P(s_2(\text{same})|s_1(R_x))$ , which is the probability that if point 1 is located in a bubble with ionization radius  $R_x$  and has temperature  $s_1$ , then point 2 is in the same heating bubble with temperature  $s_2$ . If point 1 is located at distance between  $R_{s_1}$  and  $R_{s_1} + \Delta R_{s_1}$  from the center of the sphere, then fraction of its neighbours at distance  $r$  which are outside the sphere of radius  $R_{s_2}$  and inside sphere of radius  $R_{s_2} + \Delta R_{s_2}$  can be computed. However, since bubbles can overlap, point 2 can be neutral or ionized, which leads to:

$$\begin{aligned} P(s_2(\text{same})|s_1(R_x)) &= (C(r, R_{s_1}, R_{s_1} + \Delta R_{s_1}, R_{s_2}) - C(r, R_{s_1}, R_{s_1} + \Delta R_{s_1}, R_{s_2} + \Delta R_{s_2})) \\ &\left( 1 - \sum_{R'_x} N(R'_x) \frac{4\pi}{3} R'_x{}^3 D(r, R'_x) \right) \end{aligned}$$

<sup>5</sup> Refer to footnote 3.

Therefore,

$$\begin{aligned}
\sum_{0 < s_1 < s_b} \sum_{0 < s_2 < s_b} s_1 s_2 P(s_1 \cap s_2(\text{same})) &= \sum_{R_x} N(R_x) \frac{4\pi}{3} \sum_{s_1(R_x)} \sum_{s_2(R_x)} s_1 s_2 f_b((R(s_1, R_x) + \Delta R)^3 - R^3(s_1, R_x)) \\
&\quad (C(r, R_{s_1}, R_{s_1} + \Delta R_{s_1}, R_{s_2}) - C(r, R_{s_1}, R_{s_1} + \Delta R_{s_1}, R_{s_2} + \Delta R_{s_2})) \\
&\quad \left( 1 - \sum_{R'_x} N(R'_x) \frac{4\pi}{3} R_x^3 D(r, R'_x) \right)
\end{aligned} \tag{44}$$

Now we turn to the second term on the RHS of Eq. (43).  $P(s_1 \cap s_2(\text{diff}))$  gives the probability that point 1 has temperature  $s_1$ , point 2 has temperature  $s_2$  and they both belong to different bubbles. Here we take a simple assumption that if point 2 is outside the bubble in which point 1 is, then its probability of having  $s = s_2$  is equal to the global probability of  $s_2$  temperature shell. Since point 1 and 2 can belong to bubbles of any size,

$$P(s_1 \cap s_2(\text{diff})) = \sum_{R_x} P(s_1, R_x) C(r, R_{s_1}, R_{s_1} + \Delta R_{s_1}, R_h) \sum_{R'_x} P(s_2, R'_x)$$

which gives us,

$$\begin{aligned}
\sum_{0 < s_1 < s_b} \sum_{0 < s_2 < s_b} s_1 s_2 P(s_1 \cap s_2(\text{diff})) &= \sum_{R_x} N(R_x) \frac{4\pi}{3} \sum_{s_1(R_x)} s_1 f_b((R_{s_1} + \Delta R_{s_1})^3 - R_{s_1}^3) \\
&\quad C(r, R_{s_1}, R_{s_1} + \Delta R_{s_1}, R_h) \\
&\quad \sum_{R'_x} N(R'_x) \frac{4\pi}{3} \sum_{s_2(R'_x)} s_2 f_b((R'_{s_2} + \Delta R'_{s_2})^3 - R_{s_2}^3)
\end{aligned} \tag{45}$$

Using Eqs. (41), (42), (44), and (45), we finally obtain the expression for the heating correlation function:

$$\begin{aligned}
\langle s_1 s_2 \rangle &= s_b^2 f_b - s_b^2 f_b \sum_{R_x} N(R_x) \frac{4\pi}{3} (f_b(R_h^3 - R_x^3) C(r, R_x, R_h, R_h) + R_x^3 E(r, R_x, R_h)) \\
&\quad + f_b \sum_{R_x} N(R_x) \frac{4\pi}{3} \sum_{s(R_x)} s ((R_s + \Delta R_s)^3 - R_s^3) C(r, R_s, R_s + \Delta R_s, R_h) \\
&\quad \left( 2s_b f_b + f_b \sum_{R'_x} N(R'_x) \frac{4\pi}{3} \sum_{s'(R'_x)} s' ((R'_{s'} + \Delta R'_{s'})^3 - R_{s'}^3) \right) \\
&\quad + f_b \sum_{R_x} N(R_x) \frac{4\pi}{3} \sum_{s_1(R_x)} \sum_{s_2(R_x)} s_1 s_2 ((R_{s_1} + \Delta R_{s_1})^3 - R_{s_1}^3) \\
&\quad \times (C(r, R_{s_1}, R_{s_1} + \Delta R_{s_1}, R_{s_2}) - C(r, R_{s_1}, R_{s_1} + \Delta R_{s_1}, R_{s_2} + \Delta R_{s_2})) \\
&\quad \left( 1 - \sum_{R'_x} N(R'_x) \frac{4\pi}{3} R_x^3 D(r, R'_x) \right)
\end{aligned} \tag{46}$$

We also calculate the correlation of heating at the same point ( $\langle s_1 s_1 \rangle = \langle s^2 \rangle$ ). The signal will be non-zero only if the chosen point is not heated to very high temperature. Therefore,

$$\langle s_1 s_1 \rangle = s_b^2 f_b + f_b \sum_{R_x} N(R_x) \frac{4\pi}{3} \sum_{s(R_x)} s^2 ((R_s + \Delta R_s)^3 - R_s^3)$$

This quantity is global average of  $s^2$ .

### 3.4. A Simple Model: Uniform heating

In this case we assume a limit where there is no heating profile around ionization bubble. We should get back the result derived in subsection 3.1.1.

If there are no heating shells, the second term of Eq. (35) and second and third terms of Eq. (40) can be dropped. In this limit we also obtain,  $R_h = R_x$ ,  $E(r, R_x, R_x) = D(r, R_x)$  and  $f_b = f_n$ .

Simplifying the results of section 3.3.1, 3.3.2 and 3.3.3:

$$\begin{aligned}\langle n_1 n_2 \rangle &= f_n - f_n \sum_{R_x} N(R_x) \frac{4\pi}{3} R_x^3 D(r, R_x) \\ \langle n_1 s_2 \rangle &= s_b f_n - s_b f_n \sum_{R_x} N(R_x) \frac{4\pi}{3} R_x^3 D(r, R_x) \\ \langle s_1 s_2 \rangle &= s_b^2 f_n - s_b^2 f_n \sum_{R_x} N(R_x) \frac{4\pi}{3} R_x^3 D(r, R_x) \\ \langle n_1 s_1 \rangle &= s_b f_b = s_b f_n\end{aligned}$$

The total correlation is given by:

$$\begin{aligned}\mu &= (1 + \xi)(\langle n_1 n_2 \rangle - 2\langle n_1 s_2 \rangle + \langle s_1 s_2 \rangle) - (f_n - \langle n_1 s_1 \rangle)^2 \\ &= (1 + \xi)(1 - 2s_b + s_b^2)f_n \left( 1 - \sum_{R_x} N(R_x) \frac{4\pi}{3} R_x^3 D(r, R_x) \right) - (f_n - s_b f_n)^2 \\ &= (1 - s_b)^2((1 + \xi)\langle n_1 n_2 \rangle - f_n^2)\end{aligned}$$

This expression agrees with Eq. (26) from section 3.1.1. Our model goes to correct limit for this simplified case.

Here if we take only one bubble size, we have,

$$\mu = (1 - s_b)^2 f_n ((1 + \xi)(1 - (1 - f_n)D(r, R_x)) - f_n) \quad (47)$$

### 3.5. A Simple Model: One bubble size, flat heating profile

One of the principle aims of this paper is to establish the new scales that emerge in H I correlation function for a partially heated universe. For fully heated universe ( $T_S \gg T_{\text{CMB}}$  in neutral regions), these scales are determined by the size distribution of ionized regions. In the partially heated case, there is a separation between unheated and heated neutral regions. This situation is expected to introduce new scales linked to the size of heated regions. Our detailed analysis of the physical conditions that exist during the early phase of reionization are difficult to interpret in terms of demarcated ionized, heated, and unheated regions, because unlike ionized regions which have sharp boundaries, the heated regions have shallow profiles which smoothly merge into the background. However, for the purposes of understanding our formalism we consider a simple model: a single bubble size (both ionized and heating) and the heating profile with uniform temperature (flat). Thus there are small ionization bubbles embedded in larger heated bubbles. We first ignore density fluctuations for simplicity in this section and later present the results including these perturbations. In this case, there are only three values of  $\psi = n(1 - s)$  present in the universe:  $\psi_i$ ,  $\psi_h$ ,  $\psi_b$ .  $\psi_i = 0$  since  $n = 0$  inside the ionized region. In the heated and background regions respectively,

$$\begin{aligned}\psi_h &= (1 - s_h) = 1 - \frac{T_{\text{CMB}}}{T_{\text{heat}}} \\ \psi_b &= (1 - s_{\text{bg}}) = 1 - \frac{T_{\text{CMB}}}{T_{\text{bg}}}\end{aligned}$$

If  $N$  is the number density of bubbles then the total ionized volume fraction of the universe and the heated volume fraction without correcting for overlap are respectively,

$$\begin{aligned}f_i &= \frac{4\pi}{3} R_x^3 N \\ f_{hb} &= \frac{4\pi}{3} (R_h^3 - R_x^3) N\end{aligned}$$

where  $R_x$  is the ionization bubble radius and  $R_h$  is the heating bubble radius. Allowing for overlaps, the actual heated volume fraction and the remaining non-heated volume fraction are respectively:

$$f_h = \frac{f_{hb}(1 - f_i)}{1 + f_{hb}}$$

$$f_b = 1 - f_i - f_h$$

This allows us to calculate the dimensionless temperature correlation:

$$\begin{aligned} \mu &= \langle \psi_1 \psi_2 \rangle - \langle \psi \rangle^2 \\ &= \psi_h^2 P((\psi_1 = \psi_h) \cap (\psi_2 = \psi_h)) + 2\psi_h \psi_b P((\psi_1 = \psi_h) \cap (\psi_2 = \psi_b)) + \psi_b^2 P((\psi_1 = \psi_b) \cap (\psi_2 = \psi_b)) - \langle \psi \rangle^2 \end{aligned}$$

Now we derive each term separately,

$$\begin{aligned} P((\psi_1 = \psi_h) \cap (\psi_2 = \psi_b)) &= P(\psi_1 = \psi_h) P((\psi_2 = \psi_b) | (\psi_1 = \psi_h)) \\ &= f_h f_b C(r, R_x, R_h, R_h) \end{aligned} \quad (48)$$

The other terms give:

$$\begin{aligned} P((\psi_1 = \psi_h) \cap (\psi_2 = \psi_h)) &= P(\psi_1 = \psi_h) - P((\psi_2 \neq \psi_h) \cap (\psi_1 = \psi_h)) \\ &= f_h - P((\psi_2 = \psi_b) \cap (\psi_1 = \psi_h)) - P((\psi_2 = \psi_i) \cap (\psi_1 = \psi_h)) \\ &= f_h - f_h f_b C(r, R_x, R_h, R_h) - f_i f_h C(r, 0, R_x, R_h) \\ &\quad - f_i(1 - f_i)(C(r, 0, R_x, R_x) - C(r, 0, R_x, R_h)) \end{aligned} \quad (49)$$

In Eq. (49), the third and fourth terms represent the correlation of ionized and heated regions of different bubbles and the same bubble, respectively.

$$\begin{aligned} P((\psi_1 = \psi_b) \cap (\psi_2 = \psi_b)) &= P(\psi_1 = \psi_b) - P((\psi_1 = \psi_b) \cap (\psi_2 = \psi_h)) - P((\psi_1 = \psi_b) \cap (\psi_2 = \psi_i)) \\ &= f_b - f_b f_h C(r, R_x, R_h, R_h) - f_b f_i C(r, 0, R_x, R_h) \end{aligned} \quad (50)$$

Putting the terms in Eqs. (49), (48) and (50) together, we have:

$$\begin{aligned} \mu &= \psi_h^2 (f_h - f_h f_b C(r, R_x, R_h, R_h) - f_i f_h C(r, 0, R_x, R_h) \\ &\quad - f_i(1 - f_i)(C(r, 0, R_x, R_x) - C(r, 0, R_x, R_h))) \\ &\quad + 2\psi_h \psi_b f_h f_b C(r, R_x, R_h, R_h) \\ &\quad + \psi_b^2 (f_b(1 - f_h C(r, R_x, R_h, R_h) - f_i C(r, 0, R_x, R_h)) \\ &\quad - (f_h \psi_h + f_b \psi_b)^2 \end{aligned} \quad (51)$$

If the impact of density perturbations is included, we get:

$$\begin{aligned} \mu &= (1 + \xi) [\psi_h^2 (f_h - f_h f_b C(r, R_x, R_h, R_h) - f_i f_h C(r, 0, R_x, R_h) \\ &\quad - f_i(1 - f_i)(C(r, 0, R_x, R_x) - C(r, 0, R_x, R_h))) \\ &\quad + 2\psi_h \psi_b f_h f_b C(r, R_x, R_h, R_h) \\ &\quad + \psi_b^2 (f_b(1 - f_h C(r, R_x, R_h, R_h) - f_i C(r, 0, R_x, R_h)) \\ &\quad - (\psi_b f_b + \psi_h f_h)^2 \end{aligned} \quad (52)$$

To verify the validity of our formalism, we need to consider Eqs. (51) and (52) in different limits: (a) at large scales, all the functions  $C(., ., ., .)$  tend to unity. In this case, Eq. (51) vanishes and Eq. (52) approaches the correct large scale limit (Eq. (28)), (b)  $\psi_b = \psi_h$ . In this case there is no distinction between the heated bubble and the background and we expect the correlation information from heated bubbles to disappear. In this case Eq. (52) reduces to Eq. (47), the case in which only ionized bubbles and density perturbations contribute to the correlation. One sub-case of this

scenario is when both  $\psi_b$  and  $\psi_h$  approach unity, the limit in which the entire universe is uniformly heated at high temperatures  $T_S \gg T_{\text{CMB}}$ , (c) finally, if we assume:  $R_h \rightarrow R_x$ ,  $f_h = 0$ ,  $f_b = f_n$ , we get:

$$\begin{aligned}\mu &= (1 + \xi) [\psi_b^2 f_b (1 - f_i C(r, 0, R_x, R_h))] - (\psi_b f_b)^2 \\ &= (1 + \xi) [(1 - s_b)^2 f_n (1 - (1 - f_n) C(r, 0, R_x, R_x))] - ((1 - s_b) f_n)^2 \\ &= (1 - s_b)^2 f_n ((1 + \xi)(1 - (1 - f_n) D(r, R_x)) - f_n)\end{aligned}$$

This is the same result as Eq. (47).

The agreement of our formulation with the expected results in different limits shows we have taken into account the relevant physical processes in our study.

*negative correlation:* Our formalism allows for negative correlation. Such a situation might arise if  $s > 1$  inside the heated bubble and  $s < 1$  in the background. However, we do not find many instances of negative correlation in all the cases we study here even when we neglect density correlations. As  $\xi$  is positive for all the scales we consider in this paper, inclusion of this term ensures we do not get negative correlation in any case. We check that we can generate negative correlation by assuming the centers of ionizing centers to be anti-correlated. While such a situation doesn't obtain for  $\Lambda$ CDM model, except at much larger scales, the detection of negative correlation might point to another source of the density field during EoR.

#### 4. RESULTS

The brightness temperature correlation is caused by density, ionization, and heating inhomogeneities. The main aim of this paper is to study the era dominated by heating inhomogeneities. There are two main effects in modelling the correlations in this era: (a) the near-zone effect that introduces new scales corresponding to heated bubbles around self-ionized bubbles (Figures 3 and 4). The correlation function during the partially heated era is determined by the scales of these bubbles which are much larger than the ionization bubbles. (b) the evolution of  $s = T_{\text{CMB}}/T_K$  in the far zone starting from an era where  $s$  can exceed unity.

We explore four modeling parameters in this paper: photoionization efficiency  $\zeta$ , X-ray spectral index  $\alpha$ , number of X-ray photons per stellar baryon,  $N_{\text{heat}}$ , and minimum X-ray frequency escaping the source halo  $\nu_{\text{min}}$ . These parameter have already been introduced in sections 2.1 and 2.2.  $\zeta$  is constrained by Planck results that fix the optical depth to the reionization surface;  $\zeta$  in the range 10–15 is in agreement with these results (Figure 1) (Planck Collaboration et al. (2016)). We take runs in the redshift range 10–30.

##### 4.1. Simple model

To understand the evolution of correlation function at a given scale, we first consider the simple model based on an initial bubble distribution given by an ionized bubble of a single size which is surrounded by a heating bubble of a single profile temperature (flat heating profile) with the ratio of heating to ionized bubble size remaining constant (section 3.5). We also neglect the impact of density perturbations in this case. We show the evolution of ionized, heated, and background fractions— $f_i$ ,  $f_h$  and  $f_b$ —for such a case in Figure 8. The initial radius of the ionized (heated) bubble is assumed to be 0.1 Mpc (0.7 Mpc). The initial ratio of heated and ionized fraction is the cube of the ratio of these radii. Initially nearly 90% of the universe is in the phase outside the heated bubbles. As the universe evolves, the ionized bubbles grow and so do the heated bubbles, resulting in an increase in both the ionized and heated fraction with a decrement of background fraction. This process is accompanied with an increase in the background and bubble temperature. At certain redshift, the heated bubble begin to merge driving the background fraction to zero. Eventually, the ionized fraction becomes large enough to drive the heated fraction to zero.

The evolution of correlation function (normalized using Eq. (2)) for a set of scales is shown in Figure 9<sup>6</sup>. Here the background temperature is assumed to evolve according Eq. (17) for modeling parameters:  $\zeta = 10$ ,  $N_{\text{heat}} = 1.0$  and  $\alpha = 1.5$ , while the heating bubble temperature is kept at a constant value above the background temperature. Initially the correlation function is small which is expected because the function tends to zero as  $f_i$  and  $f_h$  approach zero in the absence of density perturbations. The correlation function rises as  $f_h$  increases and then decreases again owing to multiple reasons.

<sup>6</sup> We also show the evolution of the RMS which corresponds to the plot for  $r = 0$  to guide the eye. For an experiment, the relevant quantity would be the RMS smoothed with the three-dimensional resolution of the radio interferometer, which, as discussed below could be around 3–5 Mpc for ongoing and upcoming experiments. Therefore, the measured RMS would always be smaller than the quantity shown in Figure 9.

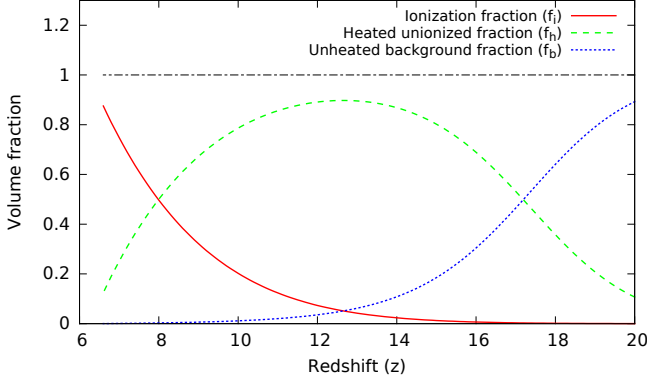


**Figure 8.** Evolution of ionized and heating fractions is shown for a fiducial model (described in the text) for  $\zeta = 10$ ,  $N_{\text{heat}} = 1$  and  $\alpha = 1.5$

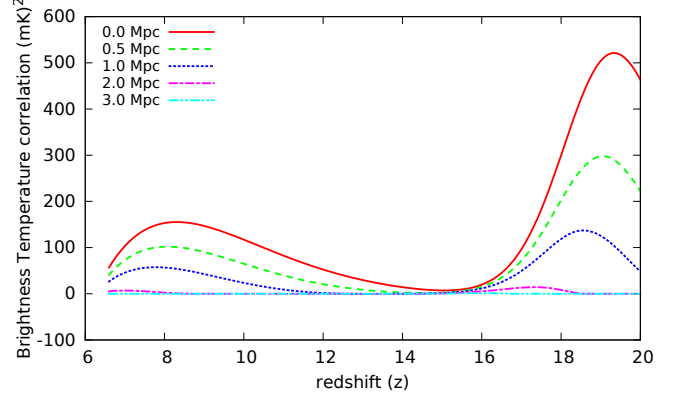


**Figure 9.** The evolution of correlation function is shown for a set of scales for the model in Figure 8.

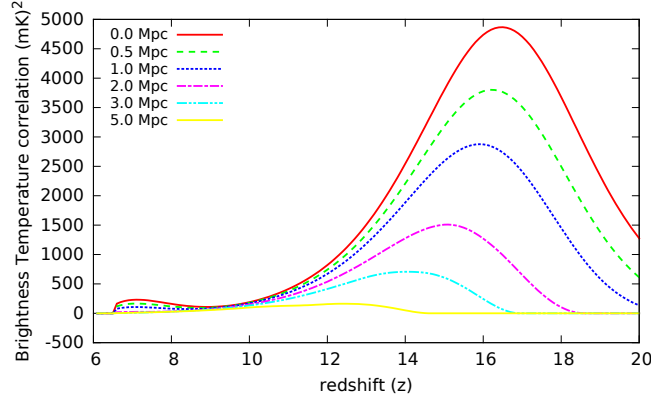


**Figure 10.** The evolution of correlation function is displayed for a set of scales for a model in which the background temperature is held constant (see text for details).

There are three distinct reasons that can wipe out information on the correlation scales generated by heating inhomogeneities: (a) increase in temperature in the heated bubbles and in the background: when these temperatures rise substantially above  $T_{\text{CMB}}$ ,  $s = T_{\text{CMB}}/T_s$  is driven to zero causing both autocorrelation of  $s$  and its cross-correlation with ionization inhomogeneities to approach zero. This is the primary cause of the evolution of the correlation function as seen in Figure 9. (b) a decrease in the gradient of temperature between the heated bubble and the background. This effect plays an important role when fuzzy boundaries of heating regions are taken into account, which we discuss in the next section. It can also be achieved when  $\nu_{\text{min}}$  is increased as seen in Figure 3. In this case, the heating inside the bubble decreases and most of the X-ray photons are used in raising the background temperature. We discuss this case in the next section, (c) merging of bubbles: this process destroys the distinction between heated bubble and background thereby erasing correlation information on the scales of the bubbles. The difference between this case and case (b) is that the latter is possible for even small heating fractions,  $f_h$ .

All these reasons play some role in determining the transition from heating to ionization inhomogeneities regime. For the parameters we consider in this paper, the effect of both (a) and (c) can be suppressed by considering a small  $N_{\text{heat}}$  while the scenario considered in (b) can be achieved by varying  $\nu_{\text{min}}$ .

This behavior is generic to all models even though the evolution on range of scales displayed in Figure 9 could change as it is determined by the sizes of heating bubbles. For instance, in Figure 9 the correlation on the scales of  $\simeq 3$  Mpc remains close to zero at all times owing to our choices of initial scales. The magnitude of correlation function is also determined by the background and heated temperatures. Both rise as the universe evolves, decreasing  $s$  and therefore decreasing the correlation function. In Figure 9,  $T_h^{-1}f_h + T_b^{-1}f_b$  reaches  $T_{\text{CMB}}^{-1}$  at  $z \simeq 16$ ; at this redshift the global H I signal vanishes and the universe makes a transition from being observable in the H I signal from absorption to emission.

However, as discussed above, the redshift at which the correlation function reaches its minimum is determined by a multitude of other causes and this transition is reached at  $z \simeq 15$ .

The minimum of correlation function around  $z \simeq 15$  signals the beginning of the phase in which the universe is uniformly heated. The signal at this time reaches nearly zero for all scales in our case because  $f_i \simeq 0.01$  at the time of heating transition and therefore ionization inhomogeneities are small and we ignore density perturbations. As ionized fraction increases, the ionization inhomogeneities start rising, reaching a peak around  $f_i \simeq 0.5$  and subsequently decline as the universe becomes fully ionized. It should be noted that the peak of the correlation function when it is dominated by ionization inhomogeneities is smaller than when it is determined by heating inhomogeneities. This is expected as  $s$  is larger than unity in the earlier phase and it is zero during the latter phase.

To isolate the impact of merging from the effect of heating on the evolution of correlation function, we show in Figure 10 a different model which is also based on the evolution of ionization and heating fractions shown Figure 8. In this case, the initial background temperature is 5 K and the temperature inside the heated bubble is 10 K and the temperatures are kept at their initial value throughout. Therefore, in this case, the heating inhomogeneities are destroyed by merging of heating bubbles and not heating, which delays the transition to uniform heating regime as compared to Figure 9.

Figures 9 and 10 allow us to identify the relevant physical processes involved in the modelling of the correlation function in the phase when heating inhomogeneities dominate, the end of this phase (owing to either heating above CMB temperature or merger), and the transition to ionization inhomogeneities domination phase. As we shall notice later, the features seen in the Figures are also present when more exact modelling is attempted. In this paper, we assume the centers of ionization bubbles to be uncorrelated. If the centers are correlated, new correlation scales can emerge, we briefly discuss this scenario later.

#### 4.2. Complete model

In this sub-section, we present results for the complete model based on the  $\Lambda$ CDM model. This generalizes the case discussed in the previous subsection in the following aspects: (a) there is a size distribution of ionization and heating bubbles (Figures 2 and 5), (b) the heating bubbles have shallow profiles (Figure 4), which makes it harder to identify the impact of sizes of heating bubbles on the correlation function.

*Dependence on modelling parameters and redshift:* In Figure 11, we show correlation functions for the complete model for different choices of modelling parameters, using Eqs. (2), (6), (16), (17), (25), (34), (38), and (46). The correlation functions shown in the Figure are large at small scales (Eq. (29)) and decrease as the distance between two points increases and approach Eq. (28) at large scales. On intermediate scales the structure of correlation function is determined by the size distribution of heated bubbles (e.g. Figure 5).

As the value of the spectral index  $\alpha$  is increased for a fixed  $N_{\text{heat}}$  there are more low frequency photons resulting in higher background temperature (Figure 3), this results in a decrease in the correlation function as it scales as  $(1 - s_b) = (1 - \langle s \rangle)$  during this phase (Eq. (28)). For the same reason, when  $N_{\text{heat}}$  is increased, the correlation decreases. Figures 12, 13 and 14 show the correlation function at different redshifts for different values of  $N_{\text{heat}}$ . At high redshifts, the correlation function is large owing to smaller background temperature. As the universe gets heated,  $s_b$  decreases reaching  $f_n$  at a certain redshift resulting in the vanishing of the correlation function at large scales (Eq. (28)). As the  $s_b$  decreases further, the impact of partial heating disappears and correlation function increases again owing to ionization inhomogeneities and H I signal is now observable in emission. We have already seen this transition for the single bubble, flat heating profile case (Figures 9 and 10). In Figure 15 we show the evolution of global H I signal for a range of parameters. The dependence of the strength and the transition from absorption to emission of the signal on different parameters is as expected from the discussion in this section.

We show the evolution of the correlation function for a range of scales in Figures 16 for different values of  $N_{\text{heat}}$  and  $\nu_{\text{min}}$ . For smaller value of  $N_{\text{heat}}$  and larger value of  $\nu_{\text{min}}$  the heating transition is delayed and the signal is larger during the era of partial heating, in line with the discussion in the foregoing; this result is in qualitative agreement with similar analyses on delayed heating, e.g. Fialkov et al. (2014).

*Correlation scales:* The scales at which we expect significant correlation are determined by the distribution of sizes of heating bubbles, whose sizes are determined by the sizes of ionization bubbles,  $R_x$ , the heating parameter  $N_{\text{heat}}$ ,  $\alpha$ , and  $\nu_{\text{min}}$  (Eq. (16)). In Figure 5, we show the size distribution of heating bubbles for a set of parameters. The heating bubble are larger than self-ionized bubbles by roughly a factor of 4.5 for this case and at  $z \simeq 14$  and the range of heating scales lie in the range 2–7 Mpc. However, as noted above, the correlation function depends on the gradient of

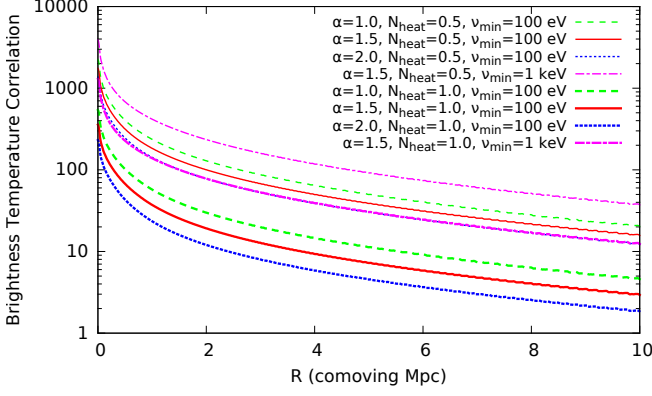


**Figure 11.** Two-point correlation functions are displayed for different values of  $N_{\text{heat}}$ ,  $\alpha$ , and  $\nu_{\text{min}}$  for  $\zeta = 10$  at  $z = 17$

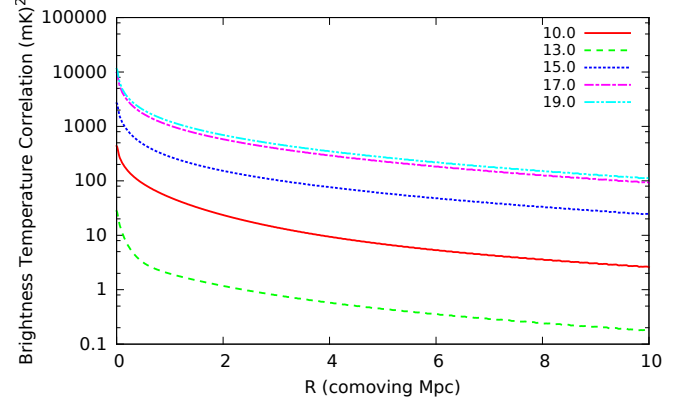


**Figure 12.** The evolution of correlation function for  $\alpha = 1.5$ ,  $\zeta = 10$ ,  $N_{\text{heat}} = 0.1$  is displayed.

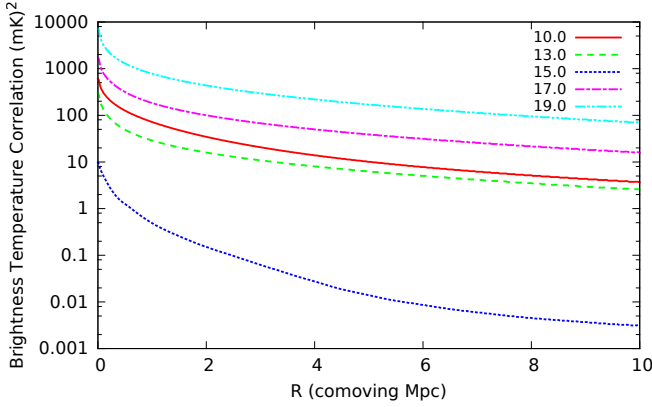


**Figure 13.** Same as Figure 12 for  $N_{\text{heat}} = 0.5$ .

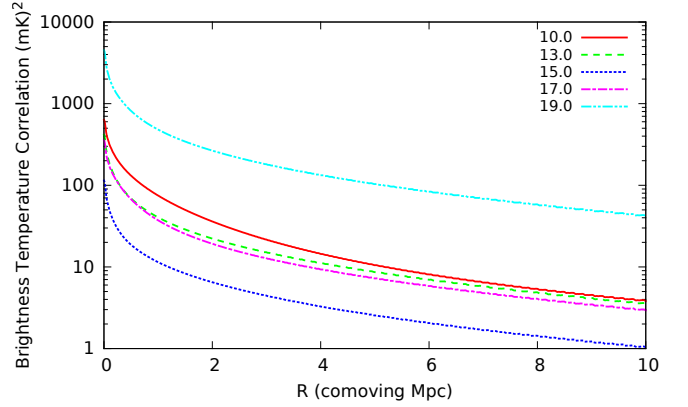


**Figure 14.** Same as Figure 12 for  $N_{\text{heat}} = 1$ .

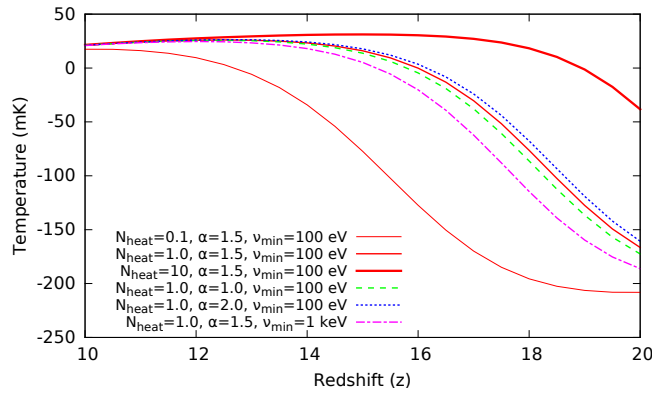


**Figure 15.** The evolution of global brightness Temperature  $\langle \Delta T_b \rangle$  (Eq. (2)) is displayed for a range of parameters for  $\zeta = 10$ .

temperature and the fuzziness of the heating bubble doesn't allow one to readily identify these scales in the correlation function.

Generically, a larger  $N_{\text{heat}}$  for a fixed  $R_x$  results in larger heating bubbles and therefore causes correlation at larger scales. An increase in  $\nu_{\text{min}}$  causes shallow heating profiles, which results in reducing the gradient of temperature between the heating bubbles and the background, thereby reducing the correlation on a given scale for the same background temperature.

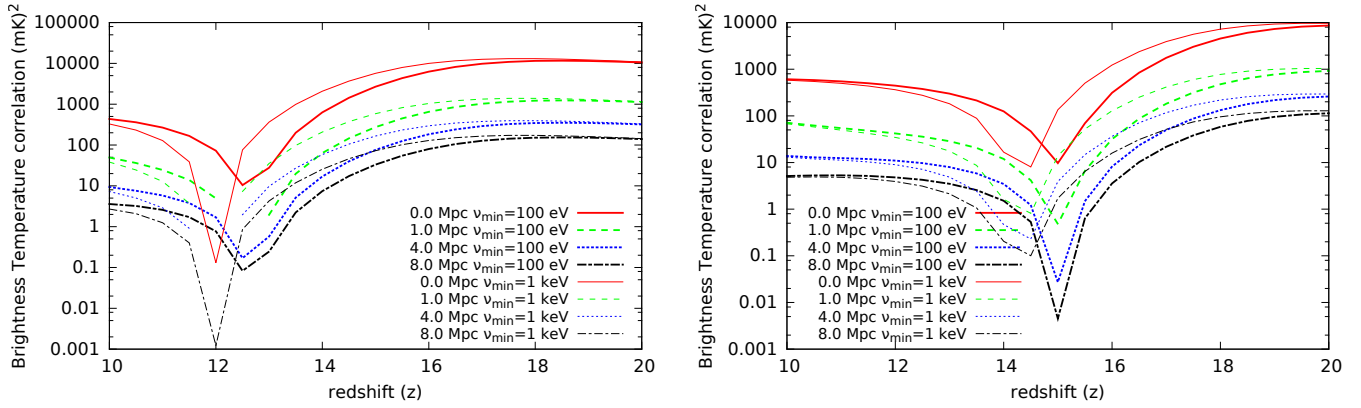


**Figure 16.** Evolution of two-point correlation function is displayed for a range of scales (including the RMS corresponding to  $r = 0$ ) for  $\alpha = 1.5$ ,  $\zeta = 10$ , and two values of  $\nu_{\min}$ . The left and right panels correspond to  $N_{\text{heat}} = 0.1$  and  $N_{\text{heat}} = 0.5$ , respectively.

In this paper, we consider a set of models in which the parameters such as  $N_{\text{heat}}$  and  $\nu_{\min}$  do not evolve. If these parameters are allowed to evolve the relation between temperature inside heating bubbles and background temperature would be more complicated. For instance, if  $R_x$  is larger at an earlier epoch owing to the evolution of  $\zeta$ , the heating bubbles could be larger causing correlations on much larger scales than shown in this paper.

*Can the merger of heating bubbles introduce new correlation scales?:* In this paper, we assume the centers of ionization bubbles to be uncorrelated. It should be noted that the positions of ionizing sources is expected to be highly correlated and this effect has already been included in the definition of self-ionized bubbles. However, the mean bubble separation corresponds to much larger scales at which the density correlation function for the  $\Lambda$ CDM model is much smaller than unity, and on such scales the H I density field is not expected to be biased with respect to the density perturbations of the dark matter. In this case the merging process is nearly homogeneous and therefore does not introduce any new scales; its main effect, as noted above, is to wipe out the correlation scales of heated bubbles. It also follows that if the centers of self-ionized bubbles are assumed to be correlated, then, in principle, correlation at much larger scales can emerge. This can occur if the H I field is highly biased with respect to the underlying density field (Ahn et al. (2015b)). We note that even though we neglect this effect for reasons given above, our formalism can easily be extended to take this effect into account.

*power spectrum, comparison with existing results, and the topology of early reionization:* The early phase of reionization has been extensively studied in the literature using semi-analytic methods but primarily large-scale simulations (e.g. Pritchard & Furlanetto (2007); Visbal et al. (2012); Tashiro & Sugiyama (2013); Mesinger et al. (2013); Fialkov et al. (2014); Ghara et al. (2015); Pacucci et al. (2014); Fialkov et al. (2017, 2015)). Most of these studies have been in the Fourier space. Our analysis suggests that real space correlation allows us to identify the physical processes more readily. Our results show that entire correlation structure in real space can be written in terms of a single function:  $C(\cdot, \cdot, \cdot, \cdot)$  and its limits given by the functions  $E(\cdot, \cdot, \cdot)$  and  $D(\cdot, \cdot)$  (section B). Fourier transform with respect the first argument  $r$  of this function yields the power spectrum.

Existing results show that, for  $k \simeq 0.1\text{--}0.5 \text{ Mpc}^{-1}$ ,<sup>7</sup> during the era of early reionization where heating inhomogeneities dominate, there is a peak in the power spectrum which is followed by a smaller peak at lower redshifts when the inhomogeneities are dominated by ionization inhomogeneities (e.g. Pritchard & Furlanetto (2007); Fialkov et al. (2014); Ghara et al. (2015)). Our results are in agreement with this general picture. They are also in agreement with analyses that have studied the impact of partial heating density perturbations at large scales (e.g. Tashiro & Sugiyama (2013); Mesinger et al. (2013))<sup>8</sup> or the impact of late heating on the fluctuating component of the signal (Fialkov et al. (2014)). Many of these analyses strongly suggest that the H I signal is a robust probe of early X-ray heating, an inference our analysis adequately captures. We also establish the dependence of the signal on different parameters, which agrees with existing results. We do not attempt a more detailed comparison with the existing results in this

<sup>7</sup> Generally a wavenumber  $k$  will contribute to a range of spatial scales; for making a comparison between real space correlation function and power spectrum, one can use the approximate conversion  $r \simeq \pi/k$ .

<sup>8</sup> At large scales, the correlation function approaches Eq. (28) which is determined by density inhomogeneities; its value could be enhanced by  $(1 - \langle s \rangle)^2$  at early times. Therefore, large scales correlation function at early times could be a reliable measure of density correlation and its statistical anisotropy, in agreement with results of Tashiro & Sugiyama (2013); Mesinger et al. (2013).

paper partly because our formulation is in real space and partly because it is hard to establish a one-to-one relation between different parameters used in the literature.

Our results are based on the assumption that the topology of the early reionization is given by Figure 6: an ionized sphere surrounded by a fuzzy heated region which merges smoothly into the background. The density perturbations determine the size of ionized regions, but the brightness temperature correlations on the scales of heating bubbles are dominated by heating autocorrelation and heating-ionization cross-correlation.

The assumption of sphericity of ionized and heating regions for the computation of correlation function is reasonable even in the presence of density perturbations because the reionization process is statistically isotropic and homogeneous<sup>9</sup>. However, the inclusion of density cross-correlation with other fields can alter the correspondence between the scale for a given set of physical parameter, e.g. the scale of heating bubble is given roughly by the distance at which the optical depth of an X-ray photon reaches unity. We retain only background density for this computation but to be more exact we need to also include the impact of density perturbations at this scale. Generally, the correlation of H I density field is small unless the H I field is highly biased with respect to the underlying density field so this correction should be small at high redshift but will become more important at smaller redshifts. Also we assume that the ionizing centers are uncorrelated, this assumption has greater validity at higher redshifts when the mean separation between the centers is larger.

While N-body simulations assume paramount importance if the H I density field at large redshifts is to be directly imaged, all of the ongoing experiments that seek to detect this signal rely upon statistical detection of this signal. Our method cannot predict the shape of individual regions but allows us to compute the statistics of the H I field. Another advantage with analytic estimates is that they are computationally inexpensive as compared to simulations. Given the uncertainty in the early heating phase of the universe, our analysis can be used to compare the observed signal for a multiple set of parameters and better understand their degeneracies at a fraction of computational cost needed to carry out an N-body simulation. For instance, the H I signal in early heating regime depends on the gradient of temperature in and across heated regions whose sizes depend on multiple physical processes. It would be of great interest to determine whether the future data can distinguish between these different physical processes.

*Detectability of the signal:* Many operational (e.g. LOFAR, MWA, PAPER, GMRT) and upcoming radio interferometers (HERA, SKA) have the capability to detect the fluctuating component of the H I signal in the redshift range  $8 < z < 25$  (for details e.g. Ahn et al. (2015a); Koopmans et al. (2015); Mesinger et al. (2014)). It is customary in the literature to present the sensitivity of radio interferometers for the detection of H I signal in terms of power spectrum, partly because the radio interferometers measure the Fourier component of the H I signal. However, these estimates can be extended to image plane (which is often a byproduct of the analysis pipeline e.g. Patil et al. (2017) for LOFAR) or real-space correlation functions used for computation of the signal in this paper (e.g. Sethi & Haiman (2008)). We discuss here the expected sensitivity of SKA1-LOW (Koopmans et al. (2015)). SKA1-LOW can detect the H I signal at  $z \simeq 16$  with a signal-to-noise varying from 100 to 10 for  $0.1 < k < 0.6 \text{ Mpc}^{-1}$  (for details see e.g. Koopmans et al. (2015)). Using  $r \simeq \pi/k$ , we expect significant detection for scales  $r \geq 5 \text{ Mpc}$  in the redshift range of interest in this paper.<sup>10</sup>

## 5. SUMMARY AND CONCLUSIONS

The main aim of this paper is to present a new analytic formalism to study the phase of EoR that is dominated by partial heating.

The main ingredients of our analytic model are: (a) correlation of the H I density field is given by the  $\Lambda$ CDM model. At large scales, this correlation dominates (Eq. (28)). (b) correlation of ionization is determined by the size distribution of self-ionized bubbles. The definition of self-ionized bubbles takes into account the clustering of halos as they form in high density regions. The cross-correlation between density and ionization inhomogeneities is neglected in our work. Both (a) and (b) have been extensively studied both analytically and numerically in the literature. (c) modelling of heating inhomogeneities using near- and far-zone around the centers of self-ionized regions. While the phase of partial heating has been studied in the literature, this formulation is new and allows us to compute the statistical quantities related to the H I signal, (d) computation of two-point correlation functions in real space for a

<sup>9</sup> We neglect redshift-space distortion in the paper which renders the density field statistically anisotropic. However, so long as the ionization and heating sources are isotropic their correlation is not affected by this anisotropy.

<sup>10</sup> Angular scale above which the H I signal can be reliably measured for most ongoing and upcoming radio interferometers is a few arcminutes;  $1'$  corresponds to nearly 3 Mpc (comoving) at  $z \simeq 15$  or these telescopes are sensitive to linear scales larger than 5–10 Mpc (comoving). However, these telescopes have frequency resolution which correspond to much smaller linear scales, e.g. MWA's frequency resolution of 40 kHz corresponds to nearly 1 Mpc (comoving) along the line of sight. Or the 3-d H I signal is probed with different resolution on the sky plane as compared to the line of sight.

sharp ionized region surrounded by a fuzzy heated bubble. We develop a formalism to compute these functions. In particular, we take into account the heating autocorrelation and heating-ionization cross-correlations while neglecting the density-heating cross-correlation. We also take into consideration both the correlation for a single bubble and for multi-bubbles, assuming the centers of self-ionized regions to be uncorrelated. We also explicitly show that our formalism reduces to the correct form in different limits (discussion following Eq. (52)). As the impact of density field is isolated in our formalism, it can readily be applied to extensions of  $\Lambda$ CDM model (e.g. Sethi & Subramanian (2009); Sarkar et al. (2016)).

We model the ionization and heating using four parameters:  $\zeta$ , which determines the ionization history of EoR and is constrained by Planck and WMAP results and three parameters to model heating— $N_{\text{heat}}$ , the number of X-ray photons per stellar baryons,  $\alpha$ , the spectral index of X-ray photons, and  $\nu_{\text{min}}$ , the lowest frequency of X-ray photons. We study the impact of these parameters on the correlation functions and find reasonable agreement with existing results.

In this paper, we assume homogeneous coupling between Lyman- $\alpha$  photons and neutral hydrogen through Wouthuysen-Field effect such that  $T_\alpha = T_K$ . As discussed in section 2.3, this is a good assumption for  $z < 20$  but we expect imperfect coupling at higher redshifts which could create inhomogeneities in the H I signal, resulting in another peak in the evolution of the signal at multiple scales (e.g. Chen & Miralda-Escudé (2008); Pritchard & Furlanetto (2007); Ahn et al. (2015a)). These inhomogeneities arise owing to the absorption of photons between Lyman- $\beta$  and Lyman-limit closer to the ionizing sources, unlike photons between Lyman- $\alpha$  and Lyman- $\beta$  discussed in section 2.3, and these inhomogeneities can be studied using formalism developed in this paper. We hope to return to this issue in the near future.

Given the uncertainty in the heating history during EoR and its impact on the H I signal, our analytic formulation allows us to isolate the impact of different physical parameters and also underline their degeneracies. Future data in the redshift range of interest,  $10 < z < 20$ , is likely to put strong constraints on the physical processes during this era. Our work is one step in the direction of understanding the data better.

## APPENDIX

### A. PROBABILITY

$$P(A|B) = \frac{P(A \cap B)}{P(B)} \quad (\text{A1})$$

$$P((A \cap B)|C) = P(A|(B \cap C)) P(B|C) \quad (\text{A2})$$

$$P(A \cap B) = P(A) - P(A \cap \tilde{B}) \quad (\text{A3})$$

### B. GEOMETRY

#### B.1. $A(R_1, R_2, d)$

Given two spheres of radius  $R_1$  and  $R_2$ , the surface area of the sphere of radius  $R_1$  that lies inside sphere of radius  $R_2$  is <sup>11</sup>:

$$A(R_1, R_2, d) = \begin{cases} 0 & d > R_1 + R_2 \\ 0 & d < R_1 - R_2 \\ 4\pi R_1^2 & d < R_2 - R_1 \\ \frac{\pi R_1 (R_2 - R_1 + d)(R_2 + R_1 - d)}{d} & \text{Otherwise} \end{cases} \quad (\text{B4})$$

where  $d$  = distance between two sphere centers.

<sup>11</sup> [mathworld.wolfram.com/Sphere-SphereIntersection.html](http://mathworld.wolfram.com/Sphere-SphereIntersection.html)  
<http://mathworld.wolfram.com/Zone.html>

B.2.  $C(x, P, Q, R)$ 

If point 1 is located between distance  $P$  and  $Q$  ( $P < Q$ ) from the center of a sphere, then  $C(x, P, Q, R)$  is the probability that its neighbour point 2 at distance  $x$  from point 1 is located outside the concentric sphere of radius  $R$ . We assume  $a$  = distance of point 1 from the center of the sphere.

- (a)  $x \leq R - Q$ : None of the neighbours of point 1 are outside the sphere of radius  $R$ , giving  $C(x, P, Q, R) = 0$ .
- (b)  $x \leq P - R$ : All the neighbours of point 1 are outside the sphere of radius  $R$ , giving  $C(x, P, Q, R) = 1$ .
- (c)  $x \geq R + Q$ : All the neighbours of point 1 are outside the sphere of radius  $R$ , giving  $C(x, P, Q, R) = 1$ .
- (d)  $R - Q \leq x \leq R - P$ : Taking  $S = R - x$ , we can see that all the neighbours of the points between distance  $P$  and  $S$  are inside the sphere of radius  $R$ . Therefore we have,

$$C(x, P, Q, R) = \left[ \frac{\frac{4\pi}{3}(S^3 - P^3)}{\frac{4\pi}{3}(Q^3 - P^3)} \right] (0) + \int_S^Q \left( 1 - \frac{A(x, R, a)}{A_x} \right) \frac{4\pi a^2}{\frac{4\pi}{3}(Q^3 - P^3)} da$$

Where,  $A_x = 4\pi x^2$  is the area of a sphere of radius  $x$ .

(d.a) If  $x \leq Q - R$ : Taking  $T = x + R$ , we see that all neighbours of points between distance  $T$  and  $Q$  are outside the sphere of radius  $R$ .

$$\begin{aligned} C(x, P, Q, R) &= \int_S^T \left( 1 - \frac{A(x, R, a)}{A_x} \right) \frac{4\pi a^2}{\frac{4\pi}{3}(Q^3 - P^3)} da + \int_T^Q \left( 1 - \frac{0}{A_x} \right) \frac{4\pi a^2}{\frac{4\pi}{3}(Q^3 - P^3)} da \\ &= \frac{Q^3 - R^3}{Q^3 - P^3} \end{aligned}$$

(d.b) Otherwise,

$$C(x, P, Q, R) = \frac{1}{2} \frac{Q^3 - (R - x)^3}{Q^3 - P^3} + \frac{3}{8x} \frac{Q^2 - (R - x)^2}{Q^3 - P^3} \left[ \frac{Q^2 + (R - x)^2}{2} + (x^2 - R^2) \right]$$

(e)  $P - R \leq x \leq Q - R$ : Taking  $S = R + x$ , we can see that all the neighbours of the points between distance  $S$  and  $Q$  are outside the sphere of radius  $R$ . Therefore we have,

$$C(x, P, Q, R) = \left[ \frac{\frac{4\pi}{3}(Q^3 - S^3)}{\frac{4\pi}{3}(Q^3 - P^3)} \right] (1) + \int_P^S \left( 1 - \frac{A(x, R, a)}{A_x} \right) \frac{4\pi a^2}{\frac{4\pi}{3}(Q^3 - P^3)} da$$

(e.a) If  $x \geq P + R$ :  $T = x - R$ , we can see that all the neighbours of the points between distance  $P$  and  $Q$  are outside the sphere of radius  $R$ . Therefore we have,

$$\begin{aligned} C(x, P, Q, R) &= \left[ \frac{\frac{4\pi}{3}(Q^3 - S^3)}{\frac{4\pi}{3}(Q^3 - P^3)} \right] (1) + \int_P^T \left( 1 - \frac{0}{A_x} \right) \frac{4\pi a^2}{\frac{4\pi}{3}(Q^3 - P^3)} da + \int_T^S \left( 1 - \frac{A(x, R, a)}{A_x} \right) \frac{4\pi a^2}{\frac{4\pi}{3}(Q^3 - P^3)} da \\ &= 1 - \frac{R^3}{Q^3 - P^3} \end{aligned}$$

(e.b) For  $x \leq P + R$ , there are two probabilities. If  $x < R - P$ , we are left with the case (d.b). Otherwise,

$$C(x, P, Q, R) = \frac{Q^3 - (R + x)^3/2 - P^3/2}{Q^3 - P^3} + \frac{3}{8x} \frac{(R + x)^2 - P^2}{Q^3 - P^3} \left[ \frac{(R + x)^2 + P^2}{2} + (x^2 - R^2) \right]$$

(f)  $R + P \leq x \leq R + Q$ : Taking  $S = x - R$ , we can see that all the neighbours of the points between distance  $S$  and  $P$  are outside the sphere of radius  $R$ . Therefore we have,

$$C(x, P, Q, R) = \left[ \frac{\frac{4\pi}{3}(S^3 - P^3)}{\frac{4\pi}{3}(Q^3 - P^3)} \right] (1) + \int_S^Q \left( 1 - \frac{A(x, R, a)}{A_x} \right) \frac{4\pi a^2}{\frac{4\pi}{3}(Q^3 - P^3)} da$$

(f.a) If  $x \leq Q - R$ :  $T = x + R$ , we can see that all the neighbours of the points between distance  $T$  and  $Q$  are outside the sphere of radius  $R$ . This is the same case as (e.a) (with  $T$  and  $S$  exchanged). Therefore we have,

$$C(x, P, Q, R) = 1 - \frac{R^3}{Q^3 - P^3}$$

(f.b) Otherwise,

$$C(x, P, Q, R) = \frac{(x-R)^3 - P^3}{Q^3 - P^3} + \frac{1}{2} \frac{Q^3 - (x-R)^3}{Q^3 - P^3} + \frac{3}{8x} \frac{Q^2 - (x-R)^2}{Q^3 - P^3} \left[ \frac{Q^2 + (x-R)^2}{2} + (x^2 - R^2) \right]$$

(g) For the last case, when  $x \geq Q - R$ ,  $x \geq R - P$ ,  $x \leq P + R$ ,

$$\begin{aligned} C(x, P, Q, R) &= \int_P^Q \left( 1 - \frac{A(x, R, a)}{A_x} \right) \frac{4\pi a^2}{\frac{4\pi}{3}(Q^3 - P^3)} da \\ &= \frac{1}{2} + \frac{3}{8x} \frac{P+Q}{P^2 + PQ + Q^2} \left[ \frac{P^2 + Q^2}{2} + (x^2 - R^2) \right] \end{aligned}$$

$$C(x, P, Q, R) = \begin{cases} 0 & x \leq R - Q \\ 1 & x \leq P - R \\ 1 & x \geq R + Q \\ \frac{1}{2} \frac{Q^3 - (R-x)^3}{Q^3 - P^3} + \frac{3}{8x} \frac{Q^2 - (R-x)^2}{Q^3 - P^3} \left[ \frac{Q^2 + (R-x)^2}{2} + (x^2 - R^2) \right] & R - Q \leq x \leq R - P, x > Q - R \\ \frac{Q^3 - R^3}{Q^3 - P^3} & R - Q \leq x \leq R - P, x \leq Q - R \\ \frac{1}{2} \frac{2Q^3 - (R+x)^3 - P^3}{Q^3 - P^3} + \frac{3}{8x} \frac{(R+x)^2 - P^2}{Q^3 - P^3} \left[ \frac{(R+x)^2 + P^2}{2} + (x^2 - R^2) \right] & |P - R| \leq x \leq Q - R, x < P + R \\ 1 - \frac{R^3}{Q^3 - P^3} & P + R \leq x \leq Q - R, \\ \frac{1}{2} \frac{(x-R)^3 + Q^3 - 2P^3}{Q^3 - P^3} + \frac{3}{8x} \frac{Q^2 - (x-R)^2}{Q^3 - P^3} \left[ \frac{Q^2 + (x-R)^2}{2} + (x^2 - R^2) \right] & R + P \leq x \leq R + Q, x > Q - R \\ \frac{1}{2} + \frac{3}{8x} \frac{P+Q}{P^2 + PQ + Q^2} \left[ \frac{P^2 + Q^2}{2} + (x^2 - R^2) \right] & R - P \leq x \leq P + R, x \geq Q - R \end{cases} \quad (\text{B5})$$

### B.3. $E(x, Q, R)$

If point 1 is inside a sphere of radius  $Q$ , then the probability that its neighbour (point 2) at distance  $x$  is outside the concentric sphere of radius  $R$  is  $E(x, Q, R)$ . We assume  $a$  = distance of point 1 from the center of the sphere.

(a)  $R > Q$  and  $x < R - Q$ : All neighbors of point 1 are inside the sphere of radius  $R$ , giving  $E(x, Q, R) = 0$ .

(b)  $R > Q$  and  $R - Q < x < R$ :  $R - x < Q$ . If  $a < R - x$ , all neighbors of point 1 are inside the sphere of radius  $R$ . For  $a > R - x$ , we can use (B4).

$$\begin{aligned} E(x, Q, R) &= \left[ \frac{\frac{4\pi}{3}(R-x)^3}{\frac{4\pi}{3}Q^3} \right] (0) + \int_{R-x}^Q \left( 1 - \frac{A(x, R, a)}{A_x} \right) \frac{4\pi a^2}{\frac{4\pi}{3}Q^3} da \\ &= \frac{1}{2} - \frac{R^3}{2Q^3} + \frac{3R^4}{16Q^3x} - \frac{3R^2}{8Qx} + \frac{3Q}{16x} + \frac{3R^2x}{8Q^3} + \frac{3x}{8Q} - \frac{x^3}{16Q^3} \end{aligned}$$

(c)  $R > Q$  and  $R < x < R + Q$ :  $x - R < Q$ . If  $a < x - R$ , all neighbors of point 1 are outside the sphere of radius  $R$ .

$$\begin{aligned} E(x, Q, R) &= \left[ \frac{\frac{4\pi}{3}(x-R)^3}{\frac{4\pi}{3}Q^3} \right] (1) + \int_{x-R}^Q \left( 1 - \frac{A(x, R, a)}{A_x} \right) \frac{4\pi a^2}{\frac{4\pi}{3}Q^3} da \\ &= \frac{1}{2} - \frac{R^3}{2Q^3} + \frac{3R^4}{16Q^3x} - \frac{3R^2}{8Qx} + \frac{3Q}{16x} + \frac{3R^2x}{8Q^3} + \frac{3x}{8Q} - \frac{x^3}{16Q^3} \end{aligned}$$

(d)  $R + Q < x$ : All neighbors of point 1 are outside the sphere of radius  $R$ , giving  $E(x, Q, R) = 1$ .

(e)  $Q > R$ ,  $x < Q - R$  and  $x < R$ :  $R - x > 0$  and  $x + R < Q$ . If  $a < R - x$ , all neighbors of point 1 are inside the sphere of radius  $R$ . If  $a > R + x$ , all neighbors of point 1 are inside the sphere of radius  $R$ .

$$\begin{aligned} E(x, Q, R) &= \left[ \frac{\frac{4\pi}{3}(R-x)^3}{\frac{4\pi}{3}Q^3} \right] (0) + \int_{R-x}^{x+R} \left( 1 - \frac{A(x, R, a)}{A_x} \right) \frac{4\pi a^2}{\frac{4\pi}{3}Q^3} da + \left[ \frac{\frac{4\pi}{3}(R+x)^3}{\frac{4\pi}{3}Q^3} \right] (1) \\ &= 1 - \frac{R^3}{Q^3} \end{aligned}$$

(f)  $Q > R$ ,  $x < Q - R$  and  $R < x < Q + R$ :  $x - R > 0$  and  $x + R < Q$ . If  $a < x - R$ , all neighbors of point 1 are outside the sphere of radius  $R$ . If  $a > R + x$ , all neighbors of point 1 are inside the sphere of radius  $R$ .

$$\begin{aligned} E(x, Q, R) &= \left[ \frac{\frac{4\pi}{3}(x-R)^3}{\frac{4\pi}{3}Q^3} \right] (1) + \int_{x-R}^{x+R} \left( 1 - \frac{A(x, R, a)}{A_x} \right) \frac{4\pi a^2}{\frac{4\pi}{3}Q^3} da + \left[ \frac{\frac{4\pi}{3}(R+x)^3}{\frac{4\pi}{3}Q^3} \right] (1) \\ &= 1 - \frac{R^3}{Q^3} \end{aligned}$$

(g)  $Q > R$ ,  $x > Q - R$  and  $x < R$ :  $R - x > 0$ . If  $a < R - x$ , all neighbors of point 1 are inside the sphere of radius  $R$ .

$$\begin{aligned} E(x, Q, R) &= \left[ \frac{\frac{4\pi}{3}(R-x)^3}{\frac{4\pi}{3}Q^3} \right] (0) + \int_{R-x}^Q \left( 1 - \frac{A(x, R, a)}{A_x} \right) \frac{4\pi a^2}{\frac{4\pi}{3}Q^3} da \\ &= \frac{1}{2} - \frac{R^3}{2Q^3} + \frac{3R^4}{16Q^3x} - \frac{3R^2}{8Qx} + \frac{3Q}{16x} + \frac{3R^2x}{8Q^3} + \frac{3x}{8Q} - \frac{x^3}{16Q^3} \end{aligned}$$

(h)  $Q > R$ ,  $x > Q - R$  and  $R < x < Q + R$ :  $x - R > 0$ . If  $a < x - R$ , all neighbors of point 1 are outside the sphere of radius  $R$ .

$$\begin{aligned} E(x, Q, R) &= \left[ \frac{\frac{4\pi}{3}(x-R)^3}{\frac{4\pi}{3}Q^3} \right] (1) + \int_{x-R}^Q \left( 1 - \frac{A(x, R, a)}{A_x} \right) \frac{4\pi a^2}{\frac{4\pi}{3}Q^3} da \\ &= \frac{1}{2} - \frac{R^3}{2Q^3} + \frac{3R^4}{16Q^3x} - \frac{3R^2}{8Qx} + \frac{3Q}{16x} + \frac{3R^2x}{8Q^3} + \frac{3x}{8Q} - \frac{x^3}{16Q^3} \end{aligned}$$

$$E(x, Q, R(Q)) = \begin{cases} 0 & x < R - Q \\ 1 - \frac{R^3}{Q^3} & R - Q < x < Q - R \\ \frac{1}{2} - \frac{R^3}{2Q^3} + \frac{3R^4}{16Q^3x} - \frac{3R^2}{8Qx} + \frac{3Q}{16x} + \frac{3R^2x}{8Q^3} + \frac{3x}{8Q} - \frac{x^3}{16Q^3} & |R - Q| < x < R + Q \\ 1 & x > R + Q \end{cases} \quad (\text{B6})$$

This can also be derived using  $E(x, Q, R) = C(x, 0, Q, R)$ .

#### B.4. $D(x, R)$

If point 1 is inside a sphere of radius  $R$ , then the probability that its neighbour (point 2) at distance  $x$  is outside the sphere is  $D(x, R)$ . We assume  $a$  = distance of point 1 from the center of the sphere.

(a)  $x < R$ : If  $a < R - x$ , then all the neighbors of point 1 are inside the sphere. For  $a > R - x$ , we can use (B4).

$$\begin{aligned} D(x, R) &= \left[ \frac{\frac{4\pi}{3}(R-x)^3}{\frac{4\pi}{3}R^3} \right] (0) + \int_{R-x}^R \left( 1 - \frac{A(x, R, a)}{A_x} \right) \frac{4\pi a^2}{\frac{4\pi}{3}R^3} da \\ &= \frac{3x}{4R} - \frac{x^3}{16R^3} \end{aligned}$$

(b)  $R < x < 2R$ : If  $a < x - R$ , then all neighbors of point 1 are outside the sphere. For  $a > x - R$ , we can use (B4).

$$\begin{aligned} D(x, R) &= \left[ \frac{\frac{4\pi}{3}(x-R)^3}{\frac{4\pi}{3}R^3} \right] (1) + \int_{x-R}^R \left( 1 - \frac{A(x, R, a)}{A_x} \right) \frac{4\pi a^2}{\frac{4\pi}{3}R^3} da \\ &= \frac{3x}{4R} - \frac{x^3}{16R^3} \end{aligned}$$

(c)  $2R < x$ : All neighbors of point 1 are outside the sphere, giving  $D(x, R) = 1$ .

$$D(x, R) = \begin{cases} \frac{3x}{4R} - \frac{x^3}{16R^3} & x < 2R \\ 1 & x > 2R \end{cases} \quad (\text{B7})$$

This can also be derived using  $D(x, R) = E(x, R, R) = C(x, 0, R, R)$ .

## REFERENCES

- Ade, P., et al. 2014, *Astron.Astrophys.*, arXiv:1303.5076
- Ade, P. A. R., et al. 2015, arXiv:1502.01589
- Ahn, K., Mesinger, A., Alvarez, M. A., & Chen, X. 2015a, *Advancing Astrophysics with the Square Kilometre Array (AASKA14)*, 3
- Ahn, K., Xu, H., Norman, M. L., Alvarez, M. A., & Wise, J. H. 2015b, *ApJ*, 802, 8
- Ali, Z. S., Parsons, A. R., Zheng, H., et al. 2015, *ApJ*, 809, 61
- Barkana, R., & Loeb, A. 2001, *Phys. Rept.*, 349, 125
- Beardsley, A. P., Hazelton, B. J., Sullivan, I. S., et al. 2016, *ApJ*, 833, 102
- Becker, R. H., Fan, X., White, R. L., et al. 2001, *AJ*, 122, 2850
- Chen, X., & Miralda-Escudé, J. 2004, *ApJ*, 602, 1
- . 2008, *ApJ*, 684, 18
- Dodelson, S. 2003, *Modern cosmology* (Academic Press)
- Fan, X., et al. 2000, *Astron. J.*, 120, 1167
- Fialkov, A., Barkana, R., & Cohen, A. 2015, *Physical Review Letters*, 114, 101303
- Fialkov, A., Barkana, R., & Visbal, E. 2014, *Nature*, 506, 197
- Fialkov, A., Cohen, A., Barkana, R., & Silk, J. 2017, *MNRAS*, 464, 3498
- Field, G. B. 1958, *Proceedings of the IRE*, 46, 240
- . 1959, *ApJ*, 129, 551
- Furlanetto, S. R., Zaldarriaga, M., & Hernquist, L. 2004a, *ApJ*, 613, 1
- . 2004b, *ApJ*, 613, 16
- Ghara, R., Choudhury, T. R., & Datta, K. K. 2015, *MNRAS*, 447, 1806
- Gnedin, N. Y., & Shaver, P. A. 2004, *ApJ*, 608, 611
- Hinshaw, G., et al. 2013, *Astrophys.J.Suppl.*, 208, 19
- Koopmans, L., Pritchard, J., Mellema, G., et al. 2015, *Advancing Astrophysics with the Square Kilometre Array (AASKA14)*, 1
- Madau, P., Meiksin, A., & Rees, M. J. 1997, *ApJ*, 475, 429
- Mesinger, A., Ewall-Wice, A., & Hewitt, J. 2014, *MNRAS*, 439, 3262
- Mesinger, A., Ferrara, A., & Spiegel, D. S. 2013, *MNRAS*, 431, 621
- Mesinger, A., Furlanetto, S., & Cen, R. 2011, *MNRAS*, 411, 955
- Morales, M. F., & Wyithe, J. S. B. 2010, *ARA&A*, 48, 127
- Natarajan, A., & Yoshida, N. 2014, *Progress of Theoretical and Experimental Physics*, 2014, 06B112
- Osterbrock, D. E. 1989, *Astrophysics of gaseous nebulae and active galactic nuclei*
- Paciga, G., Albert, J. G., Bandura, K., et al. 2013, *MNRAS*, 433, 639
- Pacucci, F., Mesinger, A., Mineo, S., & Ferrara, A. 2014, *MNRAS*, 443, 678
- Patil, A. H., Yatawatta, S., Koopmans, L. V. E., et al. 2017, *ApJ*, 838, 65
- Planck Collaboration, Adam, R., Aghanim, N., et al. 2016, *A&A*, 596, A108
- Pritchard, J. R., & Furlanetto, S. R. 2007, *MNRAS*, 376, 1680
- Pritchard, J. R., & Loeb, A. 2012, *Reports on Progress in Physics*, 75, 086901
- Rybicki, G. B., & dell’Antonio, I. P. 1994, *ApJ*, 427, 603
- Sarkar, A., Mondal, R., Das, S., et al. 2016, *JCAP*, 4, 012
- Sethi, S., & Haiman, Z. 2008, *ApJ*, 673, 1
- Sethi, S. K. 2005, *MNRAS*, 363, 818
- Sethi, S. K., & Subramanian, K. 2009, *JCAP*, 11, 021
- Shaver, P. A., Windhorst, R. A., Madau, P., & de Bruyn, A. G. 1999, *A&A*, 345, 380
- Sheth, R. K. 1998, *MNRAS*, 300, 1057
- Shull, J. M., & van Steenberg, M. E. 1985, *ApJ*, 298, 268
- Tashiro, H., & Sugiyama, N. 2013, *MNRAS*, 435, 3001
- Tozzi, P., Madau, P., Meiksin, A., & Rees, M. J. 2000, *Nuclear Physics B Proceedings Supplements*, 80, 05
- Venkatesan, A., & Benson, A. 2011, *MNRAS*, 417, 2264
- Venkatesan, A., Giroux, M. L., & Shull, J. M. 2001, *ApJ*, 563, 1
- Visbal, E., Barkana, R., Fialkov, A., Tseliakhovich, D., & Hirata, C. M. 2012, *Nature*, 487, 70
- Zaldarriaga, M., Furlanetto, S. R., & Hernquist, L. 2004, *ApJ*, 608, 622